Int. J. Nano Dimens. 2026; 17(3) : 247-270

International Journal of Nano Dimension (IJND)

https://doi.org/10.57647/ijnd.2026.1703.17

Original Research

Engineering PVA-Based Nanofibrous Mats Containing Pramipexole with Anti-Parkinsonian Effects: Fabrication, Characterization, and Pharmacological Study

Maryam Ghaffarimoghadam[1], Mitra Baghali[2], Majid Motaghinejad[3], Hakimeh Ziyadi[4,*], Danial Sadri[1]

[1]*Pharmaceutical Sciences Research Center, TeMS.C., Islamic Azad University, Tehran, Iran*
[2]*Research School of Chemistry & Applied Biomedical Sciences, Tomsk Polytechnic University, Lenin Avenue 43, 63400, Tomsk, Russian Federation*
[3]*Razi Drug Research Center, Iran University of Medical Sciences, Tehran, Iran*
[4]*Department of Organic Chemistry, TeMS.C., Islamic Azad University, Tehran, Iran*

[*]**Corresponding author:** behnazziyadi@yahoo.com

Article History

Received:
18 September 2025
Revised:
14 March 2026
Accepted:
29 April 2026
Published online:
9 June 2026
Published in Issue:
10 July 2026

Abstract:

Parkinson's disease is a progressive neurodegenerative disorder that requires long-term pharmacotherapy; however, conventional oral administration of pramipexole is associated with fluctuating plasma levels and systemic side effects. In this study, a novel electrospun PVA-based nanofibrous transdermal patch containing pramipexole was developed to enable controlled drug delivery and improved therapeutic efficacy. Pramipexole-loaded PVA and PVA/PVP nanofibers were fabricated via electrospinning and subsequently cross-linked using glutaraldehyde vapor. The nanofibrous mats were characterized in terms of morphology, wettability, rheological behavior, drug release kinetics, and in vivo neuroprotective performance. Smooth and bead-free nanofibers were obtained, confirming suitable solution viscosity and electrospinnability. Water contact angle measurements demonstrated hydrophilic behavior, with contact angles of 33° for PVA, 71° for PVA/PVP, and 43° for cross-linked PVA/PVP/Pramipexole nanofibers, indicating tunable surface wettability. *In vitro* release studies revealed an initial burst release of approximately 43% and 32% of pramipexole within 30 min for PVA and PVA/PVP nanofibers, respectively, followed by sustained release reaching ~ 52% and ~ 49% after 24 h. In contrast, cross-linked nanofibers exhibited significantly slower and more controlled drug release due to reduced polymer network permeability. Histopathological analysis of the substantia nigra region in a paraquat-induced Parkinson's disease model demonstrated a marked reduction in neuronal degeneration in both systemic and transdermal pramipexole-treated groups compared to untreated animals.

Keywords: Behavioral assessments; Nanofiber; Parkinson; Poly Vinyl Alcohol (PVA); Polyvinylpyrrolidone (PVP); Pramipexole; Transdermal mat

Cite this article: Ghaffarimoghadam M, Baghali M, Motaghinejad M, Ziyadi H, Sadri D. Engineering PVA-Based Nanofibrous Mats Containing Pramipexole with Anti-Parkinsonian Effects: Fabrication, Characterization, and Pharmacological Study. Int. J. Nano Dimens. 2026;17(3): 247-270. https://doi.org/10.57647/ijnd.2026.1703.17

1. Introduction

Nanotechnology is an emerging scientific field with its ancient history. This is well recognized that the majority of materials exhibit varied responses at various dimensions (molecular and nanometric levels) compared with their larger-scale versions. Scientists were spurred to exploit these unique properties in various disciplines [1, 2]. In the biomedical field, the implementation of nanostructures has opened up a plethora of opportunities for researchers, particularly in drug delivery, which have numerous physical, chemical, and biological attributes [3, 4, 5]. The unique characteristics of nanomaterials, such as modulated drug release, biodegradability, bio-

compatibility and enhanced cellular uptake have ignited notable interest in the development of novel drug delivery systems (NDDSs). Two crucial parameters in NDDS design that must be considered including cellular drug uptake and engagement with the biological milieu. For this purpose, a range of Nano-based systems has been reported encompassing various nanocomposites, such as nanofibers [6, 7, 8, 9]. Nanofibers made from natural polymers, as well as their hybrid and synthetic forms, exhibit remarkable properties including high porosity, ease of functionalization, large surface area, excellent encapsulation efficiency, and resistance to chemical and thermal degradation. These features make them particularly valuable in biomedical research [10, 11]. Various fabrication techniques have been employed to produce polymeric nanofibers, including the spinneret-based tunable engineered parameter (STEP) method, freeze-drying, template synthesis, phase separation, drawing, interfacial polymerization, self-assembly, and electrospinning [12, 13].

Among these, electrospinning has gained significant attention due to its simplicity, versatility, and reproducibility. This method enables the production of nanofibers with diverse architectures, such as composites, core–shell structures, net-like fibers, blends, and hybrid systems [14]. Numerous studies have explored the application of electrospun fibers in various biomedical contexts, highlighting their potential for drug delivery, tissue engineering, and other therapeutic uses. Drug delivery systems are one of the most prospective uses of electrospun fibers, particularly in their use for transdermal administration. These systems have some tremendous benefits such as the ability to reach encapsulation efficiencies of more than 100%, drug loading of up to 60%, and the potential to administer several therapeutics simultaneously [15, 16]. The fundamental principle for developing a transdermal delivery system depends on the skin's permeability characteristics. Traditional transdermal drug delivery systems (TDDSs) and patches use this property to transport drugs into the circulatory system [17]. Scientists have been encouraged to develop novel TDDSs due to a wide range of benefits such as enhanced bioavailability, increased patient acceptance, mitigation of first-pass drug degradation effects and prolonged maintenance of plasma levels leading to reduced dosing frequency and minimized side effects [18, 19]. Pramipexole is a general used anti-Parkinson's drug and a direct agonist of D2 and D3 dopamine receptors [20]. It is effective in treating symptoms of Parkinson's disease and controlling restless legs syndrome [21]. Parkinson's disease manifests with symptoms like stiffness, tremors, muscle spasms, and impaired muscle control, which pramipexole is specifically designed to treat and alleviate [22]. The drug's skin absorption has been demonstrated, leading to the development of a pramipexole skin patch as a therapeutic product.

Polyvinyl alcohol (PVA) and polyvinylpyrrolidone (PVP) are widely used in transdermal drug delivery systems and biomedical devices since they have good electrospinnability [23, 24, 25, 26]. PVP, is an amorphous synthetic polymer, holds a unique value due to high water affinity and strong adhesive character. Due to extremely high biocompatibility and lower chemical toxicity, it has found principal applications in pharmacy and biomedicine [27]. Previous research indicates that polyvinylpyrrolidone (PVP) nanofibers can enhance the rapid release of hydrophilic drugs due to their large surface area, porous structure, and good solubility in water [28]. For instance, Huang and colleagues reported that ketoprofen was released completely and almost immediately from PVP-based fibers. In contrast, the addition of ethyl cellulose (EC), a water-insoluble polymer, can slow down the drug dissolution process and extend the release period for more than 24 hours [29]. In another study, PVP/PVA nanofibrous mats were prepared as a drug carrier of buprenorphine. The results confirmed that the obtained patches can be effective for transdermal pain relief [30]. The addition of PVP was expected to enhance polymer chain entanglement and solution viscosity, thereby improving electrospinnability and promoting the formation of uniform, bead-free nanofibers [31].

Moreover, PVP incorporation allows modulation of surface wettability and polymer–drug interactions, which can influence drug distribution within the nanofibrous matrix and subsequently affect release kinetics. Such polymer blending strategies have been commonly employed to optimize nanofibrous transdermal systems by balancing hydrophilicity, structural integrity, and controlled drug release behavior [32, 33].

The present study aimed to develop and evaluate electrospun nanofibrous mats based on polyvinyl alcohol (PVA) and PVA blended with polyvinylpyrrolidone (PVP) as a novel transdermal delivery platform for pramipexole. The effect of polymer composition and glutaraldehyde vapor-phase crosslinking on the physicochemical characteristics of the nanofibers was systematically investigated using scanning electron microscopy (SEM), atomic force microscopy (AFM), Fourier-transform infrared (FT-IR) spectroscopy, and water contact angle analysis. In parallel, the *in vitro* release behavior of pramipexole from non-cross-linked and cross-linked PVA-based nanofibrous systems was quantitatively evaluated using high-performance liquid chromatography (HPLC). To assess the therapeutic relevance of the developed system, the neuroprotective efficacy of transdermal pramipexole nanofibers was further compared with conventional systemic administration through behavioral, biochemical, and histopathological evaluations in a paraquat-induced Parkinson's disease mouse model. Figure 1 provides a schematic overview of the overall experimental design and workflow of the study.

2. Experimental

2.1 Materials

Pramipexole was purchased from Abidi Pharmaceutical Company, Iran. Polyvinyl alcohol (PVA; molec-

https://doi.org/10.57647/ijnd.2026.1703.17

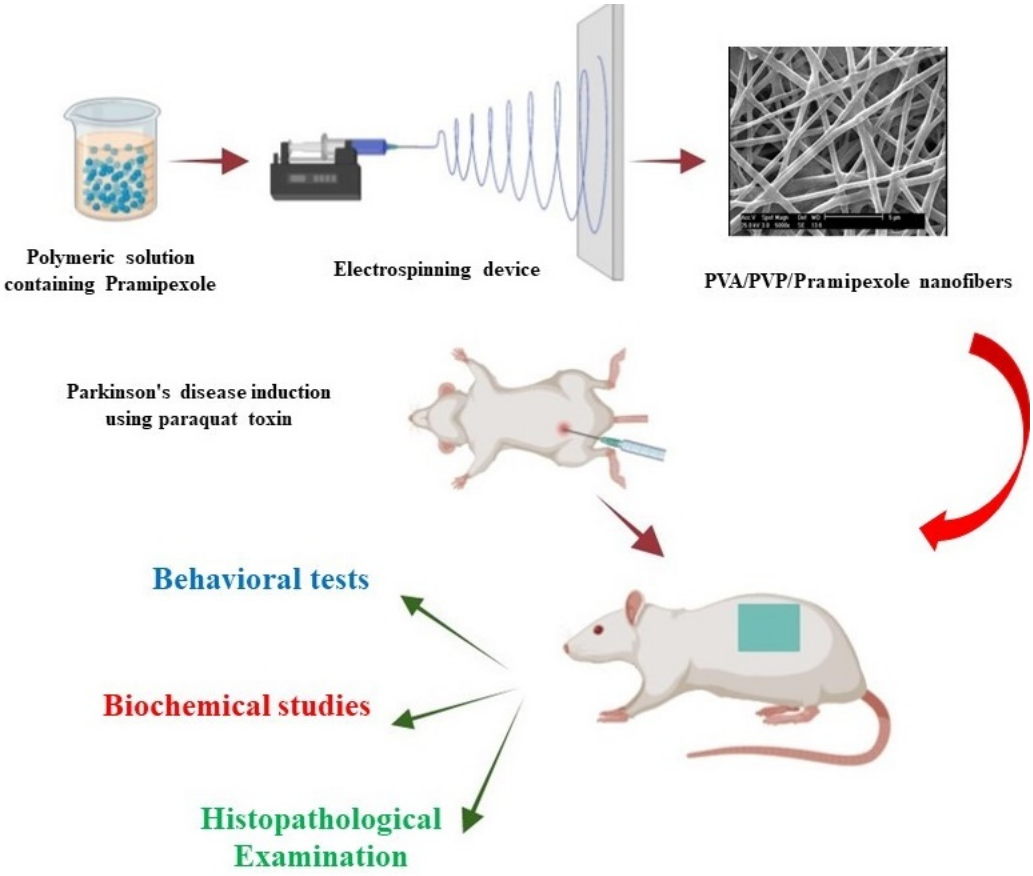

Figure 1. schematic description of research.

ular weight 88,000 g/mol, 88% hydrolyzed) and polyvinylpyrrolidone (PVP; K-90 grade, molecular weight 360,000 g/mol) were sourced from Merck Chemical Co. Phosphate-buffered saline (PBS) and glutaraldehyde solution (25% in water, density 1.06 g/cm^3) were purchased from Titrachem Company. Paraquat toxin was bought from shimi sabz jonoub company, Iran. Deionized water was obtained from the house and was used in all the process.

2.2 Animals

32 male Syrian rats weighing between 35-30 grams were used, divided into four groups of eight. The rats were obtained from the animal holding facility of the Iran University of Medical Sciences. They were housed in specialized cages under controlled conditions of temperature, humidity, and lighting, with unlimited access to water and specific mouse food. They were maintained for one week prior to the start of the experiments.

2.3 Methods

2.3.1 Preparation of PVA nanofibers and PVA nanofibers containing pramipexole

PVA solution (10% w/v) was prepared by dissolving 1.2 g of PVA in deionized water and was stirred for 3 h at 50 °C to obtain a homogeneous solution. The prepared solution was then injected to the electrospinning device to obtain PVA nanofibers. After that, PVA solution containing Pramipexole was obtained by adding 100 mg of drug to PVA solution (10% w/v) and stirred for 30 min at 30 °C. The electrospinning operation was conducted using an Electrospinning machine (FNM Ltd., Iran, www.fnm.ir) at room temperature. A 5-mL syringe fitted with an 18-gauge needle was employed to electrospin the prepared solutions. For this study, the optimal electrospinning conditions were identified as an applied voltage of 20 kV, a feeding rate of 0.5 mL/h, and a nozzle-to-collector distance of 10 cm.

2.3.2 Preparation of PVA/PVP nanofibers and PVA/PVP nanofibers containing pramipexole

For the preparation of the nanofibrous mats, an equal weight ratio of PVA and PVP powders was utilized, specifically in a 50/50 (w/w) configuration. To begin the process, 0.6 g of PVA powder were dissolved in 12 mL of deionized water. This mixture was stirred thoroughly at a temperature of 50 °C until a clear and transparent solution was achieved, indicating that the PVA had fully dissolved. Subsequently, 0.6 g of PVP powder were gradually added to the prepared PVA solution. The combination was stirred continuously to ensure that the two substances mixed thoroughly and formed a homogeneous solution, which is crucial for the quality and consistency of the resulting nanofibrous mats. This meticulous approach ensures that the final product exhibits the desired properties for its intended applications. Next, PVA/PVP solution was contained pramipexole by slowly adding 100 mg of drug to the 50/50 w/w PVA/PVP solution

and stirred for 3 min at 30 °C. All prepared solutions were injected into the electrospinning device under the following condition: a voltage of 20 kV, a flow rate of 0.5 mL/h, and a nozzle-to-collector distance of 10 cm.

2.3.3 Cross-linking of electrospun nanofibrous mats

Cross-linking of the electrospun PVA/Pramipexole and PVA/PVP/Pramipexole nanofibrous mats was performed using glutaraldehyde vapor-phase treatment to enhance structural stability while preserving the fibrous morphology. Briefly, the electrospun mats (30 × 15 cm) were placed inside a sealed desiccator containing an open vial of aqueous glutaraldehyde solution (25% w/w) as the vapor source. The nanofibrous mats were positioned above the solution without direct contact to avoid fiber fusion or structural collapse. The desiccator was maintained at room temperature, allowing controlled diffusion of glutaraldehyde vapor into the nanofiber matrix. The exposure time was set to 24 h to ensure sufficient cross-linking through the formation of acetal bonds between the hydroxyl groups of PVA and glutaraldehyde molecules. After vapor treatment, the cross-linked mats were removed and vacuum-dried for 4 h to eliminate residual glutaraldehyde and moisture. This vapor-phase cross-linking approach was selected instead of solution immersion to minimize excessive swelling, preserve porosity, and reduce residual cytotoxicity, making the nanofibrous mats more suitable for transdermal biomedical applications. The successfully cross-linked mats were subsequently used for physicochemical characterization, in *vitro* drug release studies, and pharmacological evaluations.

2.4 Measurements and characterization

The characteristics of the obtained nanofibers was investigated using SEM (Philips XL 30 and S-4160). For this purpose, samples were cut in 1.5 × 0.5 cm dimensions and coated with gold. In the following, the diameters of the nanofibers were determined by analyzing 20 randomly selected fibers from SEM images (10 × 10 µm) using microstructure measurement software, and diameter distribution charts were created using Origin software. The Fourier transform infrared (FTIR) spectra of the nanofibers were obtained using a Shimadzu S 8400 Fourier transform infrared spectrophotometer. The spectra were recorded within the 400 – 4000 cm^{-1} range with a resolution of 2 cm^{-1}. The surface hydrophilicity of the nanofibers was assessed using contact angle measurements with Veho USB Microscope. For analyzing the surface properties of the mats, AFM device (NT-MDT model TD150) was used. The viscosities were measured using the Brookfield DV-3 viscometer. All experiments were carried out three times at ambient temperature.

2.5 *In vitro* dissolution study

2.5.1 Pramipexole standard solutions

To assess the drug release behavior, a calibration curve was generated using pramipexole standard solutions. The buffer was prepared by dissolving two PBS tablets in one liter of distilled water, producing a 0.1 M phosphate-buffered saline (PBS) solution. From this medium, 2 mg of pramipexole was first dissolved in 10 mL PBS and subsequently transferred to a 100 mL volumetric flask, where the volume was adjusted with PBS to obtain the stock solution. Serial dilutions of this stock were then prepared to yield concentrations between 0.5 and 30 ppm. These solutions were analyzed with a HPLC system operated at 288 nm. The calibration curve was established by plotting HPLC peak areas against corresponding concentrations, providing a reliable reference for evaluating drug release kinetics and the performance of the nanofiber carriers.

2.6 High-performance liquid chromatography (HPLC)

The concentration of pramipexole in each sample was quantified using high-performance liquid chromatography (HPLC) on a Yaunglin Co. 9100 system equipped with a reversed-phase C18 column (250 × 4.6 mm, 5 µm particle size). The analytical method was optimized in accordance with the United States Pharmacopeia (USP) guidelines for pramipexole to ensure reliable and accurate quantification. The mobile phase consisted of acetonitrile, methanol, and buffer in a volume ratio of 67:30:3 (v/v/v) and was delivered at a constant flow rate of 1.0 mL/min under isocratic conditions. The buffer solution was prepared by dissolving 6.8 g of potassium dihydrogen phosphate (KH_2PO_4) in 1 L of distilled water, followed by pH adjustment to 7.5 using potassium hydroxide. The solution was filtered and sonicated for 5 min prior to use to remove particulate matter and dissolved gases. The detection wavelength was set at 263 nm, corresponding to the maximum absorbance of pramipexole, and the column temperature was maintained at 25 °C throughout the analysis. Prior to sample injection, the HPLC column was equilibrated with the mobile phase to ensure stable baseline conditions. A calibration curve (figure 2) was constructed using standard pramipexole solutions prepared in phosphate buffer solution (PBS, pH 7.4) over a concentration range of 1–50 µg/mL. The calibration plot exhibited excellent linearity with a correlation coefficient (R^2 = 0.998). All measurements were performed in triplicate, and the results are reported as mean ± standard deviation.

2.7 *In vitro* release study

The *in vitro* release behavior of pramipexole from PVA and PVA/PVP nanofibers was assessed using the dissolution method. In this case, phosphate-buffered saline solution was used as the optimal buffer. Each two PBS tablets were dissolved in 1000 mL of distilled water, and 900 mL of this solution was filled into each cell of the dissolution apparatus (Noavaran Co., Iran) and the electrospun nanofiber mats were cut into small pieces and placed in a paddle dissolution device at temperature 37 ± 0.5 °C with stirring rate at 100 rpm. Samples were collected at 5, 10, 20, and 30 minutes, followed by additional time points at 1, 2, 6, 24, and 48 hours. Each 5 mL sample was immediately replaced with fresh PBS buffer

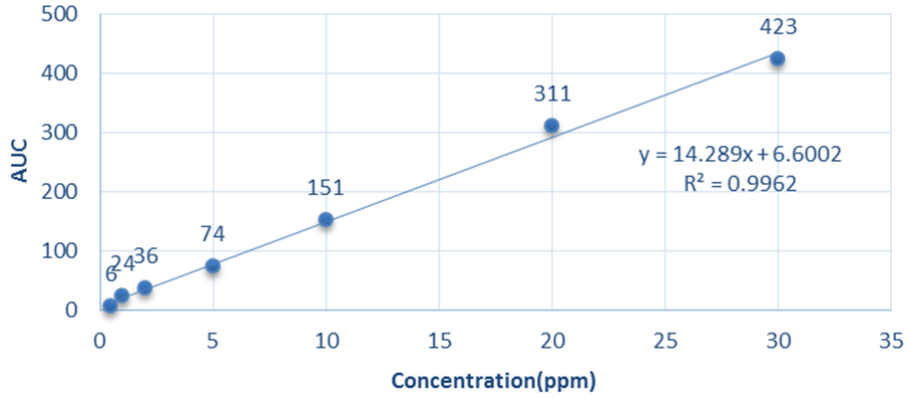

Figure 2. Calibration curve of pramipexole hydrochloride in phosphate buffer pH = 7.4.

to maintain consistent conditions. After collecting the samples, a filtration process was performed to prepare them for analysis, and the concentration of pramipexole was assessed using HPLC. The drug content was subsequently calculated based on a formula derived from the established standard calibration curve, allowing for a precise determination of pramipexole levels. The data regarding drug release was represented as a percentage of pramipexole released, with complete release (100%) reflecting the total amount of drug originally embedded within the nanofibers. To ensure the findings were both reliable and accurate, each experiment was conducted in triplicate, allowing for validation of the results. Additionally, control samples and calibration standards were incorporated into the study to minimize any potential analytical variability, further enhancing the precision of the measurements. This comprehensive approach not only strengthens the credibility of the data obtained but also provides valuable insights into the release kinetics of pramipexole, which is crucial for evaluating its therapeutic efficacy and potential applications in drug delivery systems.

2.8 Stability of nanofibers

The PVA/PVP/Pramipexole nanofibers obtained by electrospinning were cut into 8 pieces of 1.5 × 0.5 cm and placed in 8 separate containers containing PBS at four specified time intervals. After the specified times, the samples were taken out of the solution, dried under vacuum, and then subjected to SEM imaging.

2.9 Pharmacological method

2.9.1 *In vivo* rat studies and Parkinson's disease induction method

An *in vivo* animal investigation was conducted to assess the efficacy of the PVA/PVP/Pramipexole nanofiber mat in reducing Parkinson's disease symptoms in Syrian rats. Prior approval from the Animal Ethics Committee of Islamic Azad University Tehran Medical Sciences was obtained for all animal experiments. (Ethics No. IR.IAU.PS.REC.1398.220). After a week of acclimatization, 32 male Syrian mice were divided into four separate groups: First group, received normal saline and was considered as the control group. Second group, received paraquat toxin and was treated with Pramipexol orally (systemic). Third group, received paraquat toxin and was treated with transdermal nanofiber patch containing Pramipexole and the last group, received paraquat toxin without any treatment. To initiate the Parkinson's disease model, rats in groups 2, 3, and 4 received weekly intraperitoneal injections of paraquat toxin at a dosage of 10 mg/kg for four consecutive weeks.

2.9.2 Treatment with pramipexole drug and nanofibrous mat

After four weeks of paraquat toxin injection, the second group underwent a 10-day treatment with a dose of 0.3 milligrams of pramipexole administered orally. The third group received the same medication dosage after depilation of the dorsal body surface and application of a skin patch (Fig. 3 (a,b)). The fourth group served as the untreated control and did not receive any medication.

2.10 Behavioral tests

Standard behavioral assessments were administered to evaluate motor impairments in animals after completing the ten-day treatment period.

2.10.1 The open field test

This test is utilized to measure movement disorders, anxiety, depression, explorative and stereotypical behaviors in rodents [34]. The open field consists of a quiet and tranquil room containing a Plexiglas chamber measuring 40 × 40 × 30, divided into 16 equal squares on the floor. The animals were introduced to the testing environment at least one hour prior to the experiment. To familiarize the animals with the apparatus, they were placed in it for 10 minutes one day before the actual test. The next day, each animal was positioned in the central square of the apparatus and observed for 5 minutes to evaluate their behavior, including the frequency of staying in the center or periphery and the number of movements.

2.10.2 Rotarod test

To assess motor coordination and balance ability, the rotarod test was conducted [35]. For this purpose, the rats were positioned on a Rotarod device (TSE Rotarod

(a) (b)

Figure 3. (a) The intraperitoneal injection of paraquat toxin, and (b) The group receiving pramipexole through a skin patch.

System) with adjustable rotational speed. The initial rotation speed of the rod was set at 5 revolutions per minute (rpm), which was then gradually increased to 21 rpm over a duration of 300 seconds (5 minutes). The target speed of 21 rpm served as the primary measure for assessing balance across all groups. Prior to conducting the test, the animals underwent a familiarization phase. Subsequently, each mouse was evaluated three times within a single day, with an interval of 45 minutes between each assessment, and the average time was calculated.

2.10.3 Catalepsy activity

The bar method, as outlined by Wadenberg et al., was employed to assess the symptoms of catalepsy [36]. The test involves utilizing a fixed bar with a platform. The bar was positioned 4 cm above the platform and had a diameter of 4 mm. During the experiment, the animal was placed on the platform, and its paws were placed on the bar in a controlled manner. The amount of time the animal maintained this position was measured using a stopwatch and has considered as the bar test duration. The test concluded when the animal removed one or both paws from the bar or began to move its head in an exploratory manner.

2.11 Biochemical studies

At the end of the tenth day of treatment and following behavioral assessments of the animals, each animal group was anesthetized with a dose of 50 mg/kg of Thiopental. Subsequently, their brains were removed, and the substantia nigra (black substance) was isolated using the stereotaxic technique for the evaluation of parameters related to oxidative stress, inflammation, and apoptosis.

2.11.1 Determination of oxidative stress, apoptotic markers and brain inflammatory mediators

The levels of four oxidative stress markers (Superoxide Dismutase (SOD), Glutathione Peroxidase (GPx), Malondialdehyde (MDA) and Glutathione Reductase (GR)), Apoptotic Markers (Bax and Bcl-2) and Inflammatory Mediators (Tumor necrosis factor alpha (TNF-alpha) and Interleukin 1 beta (IL-1 Beta)) were assessed in midbrain homogenates using specialized Research ELISA kits (PASARGAD, IRAN) following the provided instructions. The midbrain portion was isolated and treated with PBS (pH 7.4) through sonication. After centrifugation, the supernatant was collected. A volume of forty microliters of the sample was initially placed into the test wells, followed by the addition of specific antibody and Streptavidin-HRP. Subsequently, the sealing membrane was applied, and the mixture was gently shaken and incubated at 37 °C for 60 minutes.

2.12 Histopathological examination

Brain tissue samples were promptly removed from all groups, diced into small fragments, and preserved in 10% buffered formalin for a duration of 24 hours. Subsequently, the tissue fragments were rinsed, dehydrated using alcohol, cleansed with xylene, and embedded in paraffin in a hot-air oven at 56 °C for 24 hours. Histopathological examination involved slicing serial sections of approximately 4 µm thickness, which were then stained with hematoxylin and eosin [37]. To ensure impartiality, all steps of histopathologic processing and evaluation were conducted by a qualified observer who remained unaware of the experimental groups. The tissue sections were subsequently examined using a light microscope (Nikon microscope ECLIPSE E400, Japan) to assess any histopathological alterations.

3. Results and discussions

3.1 Characterization

Electrospun nanofibers have gained considerable emphasis as drug delivery systems due to their unique functional properties and very simple fabrication methods [38]. The main aim of this work is to develop novel electrospun polymeric nanofibers for the treatment of Parkinson's disease as a carrier of pramipexole and investigate the pharmacological properties. Drug-loaded nanofibers were developed by an electrospinning technique using biocompatible polymers. In order to find the optimal conditions of electrospinning and a suitable carrier for delivering pramipexole, the electrospinning of PVA and

PVP polymers was investigated under various conditions. As previously mentioned, four distinct solutions were prepared: a pure PVA solution, a drug-loaded PVA solution, a pure PVP solution, and a drug-loaded PVP solution. These solutions were subsequently introduced into the electrospinning apparatus, maintaining the conditions established in our prior research [30]. Specific parameters included a nozzle-to-collector distance of 10 cm, an applied voltage of 20 kV, and a flow rate of 0.5 mL/h. Upon the successful completion of the electrospinning process and the formation of nanofibers, the morphology of the resulting samples was meticulously analyzed using scanning electron microscopy (SEM). This analysis was conducted to evaluate critical aspects such as fiber diameter, uniformity, and surface characteristics. Such detailed morphological assessments are essential for understanding the physical properties of the electrospun fibers, as they can significantly influence the performance and drug release behavior of the final nanofibrous mats. Moreover, accurate characterization contributes to the development of optimized materials for various biomedical applications.

Figure 4 (a) presents the morphology and corresponding histogram of PVA nanofibers, revealing a uniform structure with a seamless surface texture and an average fiber diameter of 161 nm ± SD. The SEM analysis of PVA/Pramipexole is shown in Fig. 4 (b). As can be seen, the image confirms the bead-less, uniform and smooth formation of PVA/Pramipexole nanofibrous mat. Additionally, by analyzing the histogram of nanofibers, the addition of drug increased the mean diameter of nanofibers to 187 nm ± SD.

Following glutaraldehyde vapor-phase cross-linking, the PVA/Pramipexole nanofibers (Fig. 4 (c)) preserved their fibrous architecture without fiber fusion or collapse. A moderate increase in average fiber diameter to 211 nm ± SD was observed, which is attributed to the gradual absorption of glutaraldehyde vapor into the nanofiber matrix and the formation of acetal cross-links between PVA hydroxyl groups. Importantly, the vapor-phase treatment-maintained porosity and fiber integrity, confirming its suitability for biomedical applications. Therefore, it can be concluded that vapor treatment using glutaraldehyde is an effective method for cross-linking PVA/Pramipexole nanofibers. In the following, PVA/PVP composite nanofibers and PVA/PVP composite nanofibers containing pramipexole were prepared by the electrospinning of PVA/PVP solution with the ratio of 50/50 W/W (optimal concentration according to our previous research [30]) and the same condition of electrospinning process for PVA. In all samples, SEM images (Fig. 4 (d,e)) revealed the formation of narrow, homogenous and smooth fibrous meshes with no beads and adhesion. The diameter distribution analysis revealed that the average diameters of PVA/PVP and PVA/PVP/Pramipexole nanofibers were 104 nm ± SD and 231 nm ± SD, respectively. It is evident that incorporating PVP into the PVA solution reduces the nanofiber diameter, whereas the addition of pramipexole results in thicker PVA/PVP nanofibers. This increase in fiber diameter can be attributed to the enhanced conductivity of the solution and the resulting nanofibers, which influence the electrospinning process and lead to larger-than-expected fiber formation [39]. Although PVA is known as a non-toxic and cheap biocompatible carrier, its high solubility in water and significant hydrophilicity are one of its disadvantages for controlled drug release. To address these issues, PVA/PVP cross-linking methods are used to reduce hydrophilicity. Several methods have been used to crosslink PVA/PVP, including the citrate method, glutaraldehyde liquid, etc. Among these methods, glutaraldehyde vapor treatment stands out as a desirable method due to the lack of direct contact with the chemical substance. The glutaraldehyde vapor-cross-linked PVA/PVP/Pramipexole nanofibers (Fig. 4 (f)) retained a homogeneous and porous fibrous structure with no evidence of fiber melting or adhesion. The average fiber diameter increased to 252 nm ± SD, which can be explained by controlled vapor diffusion and cross-link formation within the fibers. Compared to non-cross-linked counterparts, the cross-linked nanofibers demonstrated enhanced structural stability, which is critical for maintaining integrity during prolonged exposure to aqueous environments [40, 41]. Electrospun 10% PVA, 10% PVP, non-cross-linked and cross-linked PVA/PVP (1:1) containing pramipexole under optimally predefined conditions produced fibers with bead-less, uniform and smooth surface. Therefore, this morphology can be attributed to the properties of the solutions that offer low surface tension, high miscibility, suitable viscosity and high conductivity, all of which the nanofiber production requires [42]. Moreover, representative SEM images of nanofibers containing drug are smooth and uniform and no visible drug crystals were found on or near the surface.

Additionally, Fig. 5 (a,b,c) presents scanning electron microscopy (SEM) images of the cross-linked PVA/PVP/Pramipexole nanofibrous mat, clearly demonstrating the effective positioning of the nanofibers on the surface of the fabric. For this purpose, a polyester fabric was tightly wrapped around the rotating drum collector of the electrospinning apparatus, and the nanofibrous mats were directly deposited onto the fabric substrate during the electrospinning process. This visualization is critical for further investigations, as it provides valuable insight into the distribution and arrangement of the nanofibers, which can significantly influence their functional performance in drug delivery applications. These findings underscore the potential of the cross-linked nanofibrous mats in biomedical contexts, paving the way for innovative applications in drug delivery systems. The well-defined structure and controlled fiber distribution can improve the release kinetics of pramipexole while enhancing the stability and efficacy of the drug over time. Furthermore, the porous nature of the nanofibers may facilitate better interaction with biological systems, thereby increasing the therapeutic outcomes.

It is important to evaluate the stability of nanofibers in PBS solution for their application as biomaterials

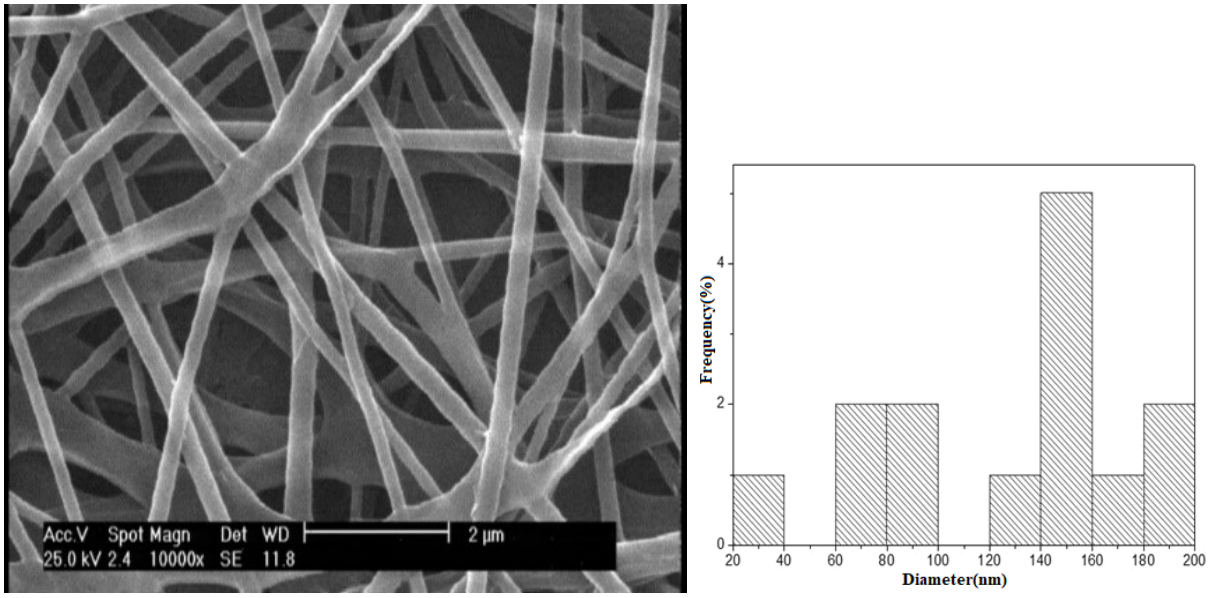

(a)

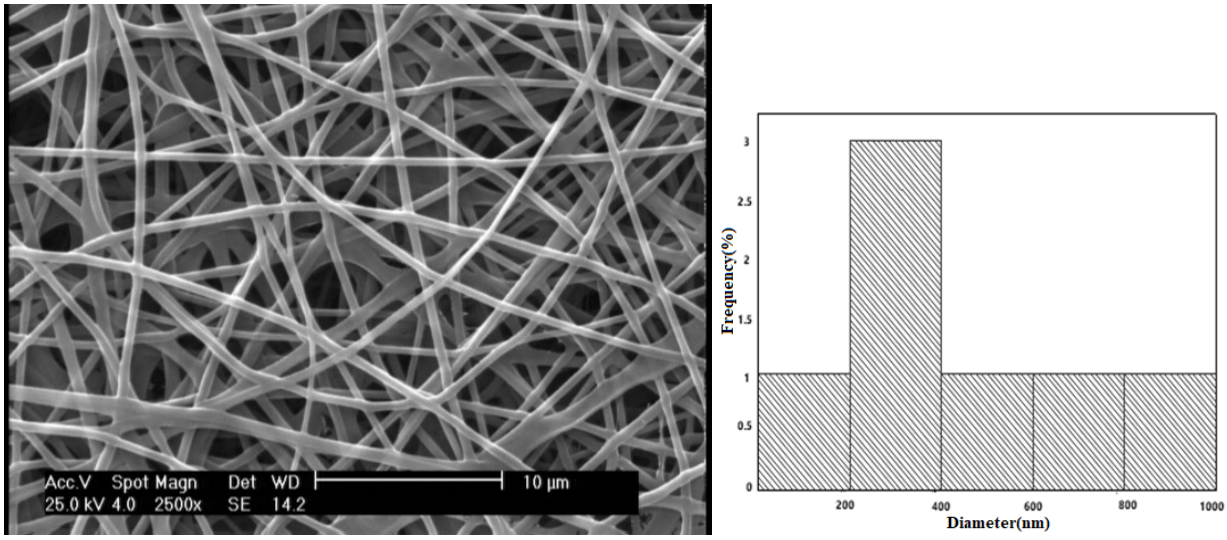

(b)

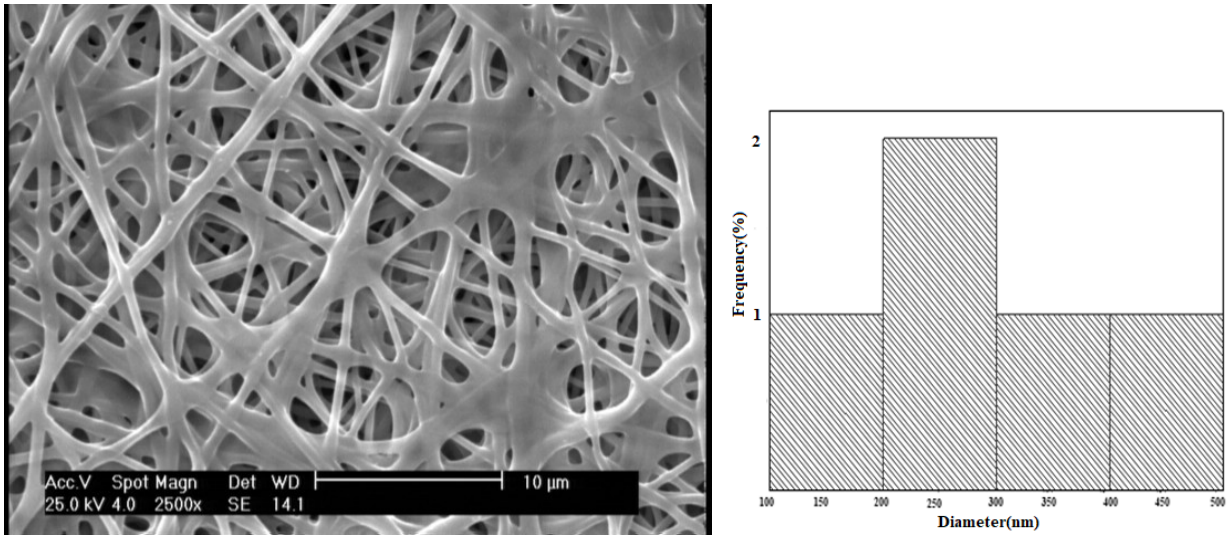

(c)

https://doi.org/10.57647/ijnd.2026.1703.17

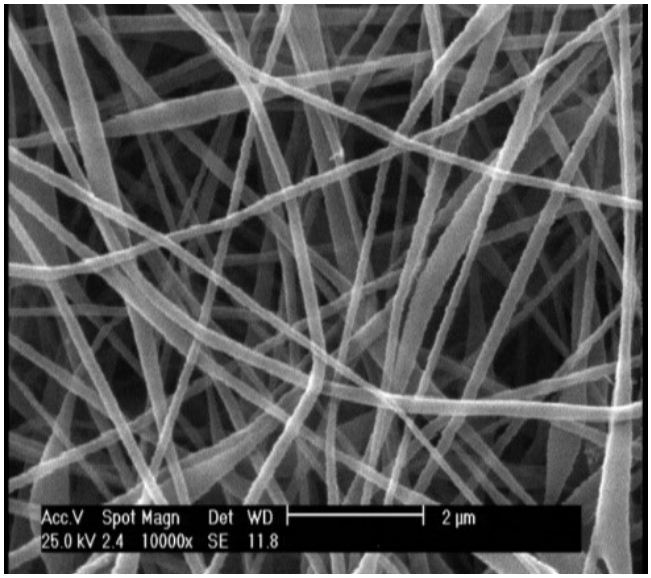

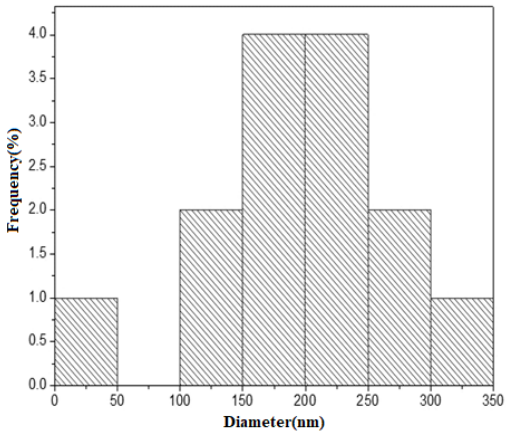

(d)

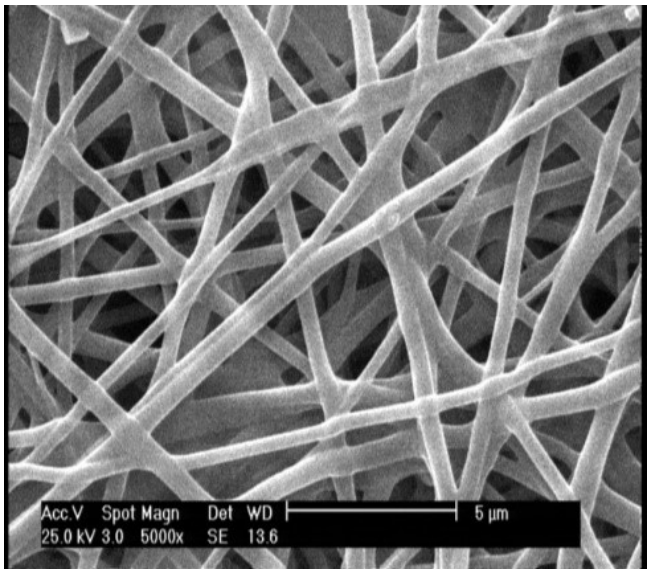

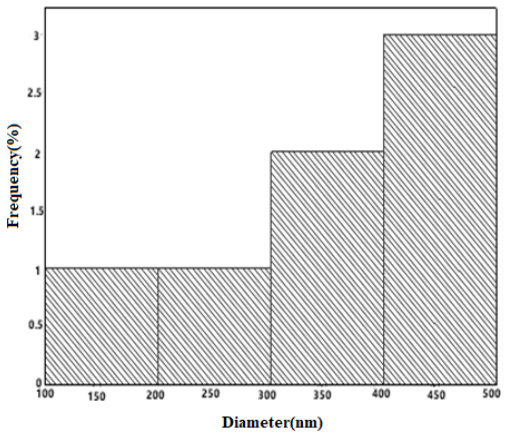

(e)

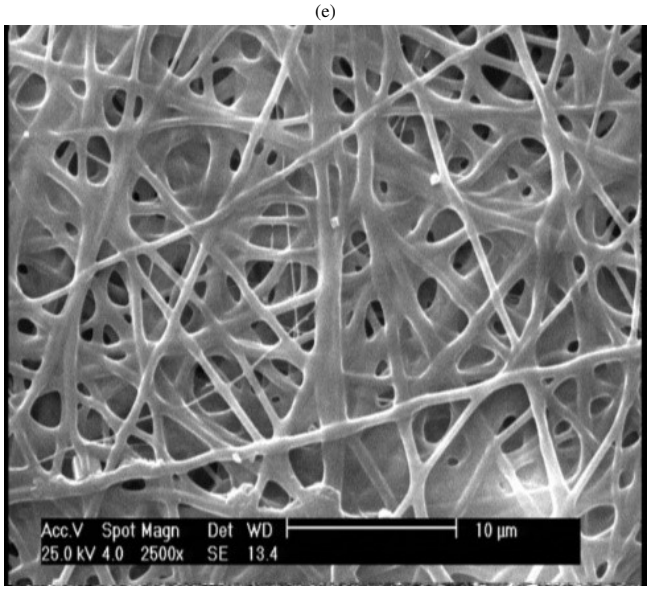

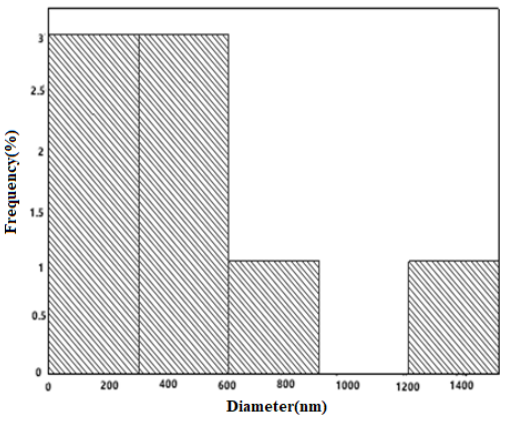

(f)

Figure 4. SEM images and fiber diameter distribution of (a) PVA nanofibers, (b) PVA/Pramipexole nanofibers, (c) cross-linked PVA/Pramipexole nanofibers, (d) PVA/PVP nanofibers, (e) PVA/PVP/Pramipexole nanofibers and (f) cross-linked PVA/PVP/Pramipexole nanofibers.

https://doi.org/10.57647/ijnd.2026.1703.17

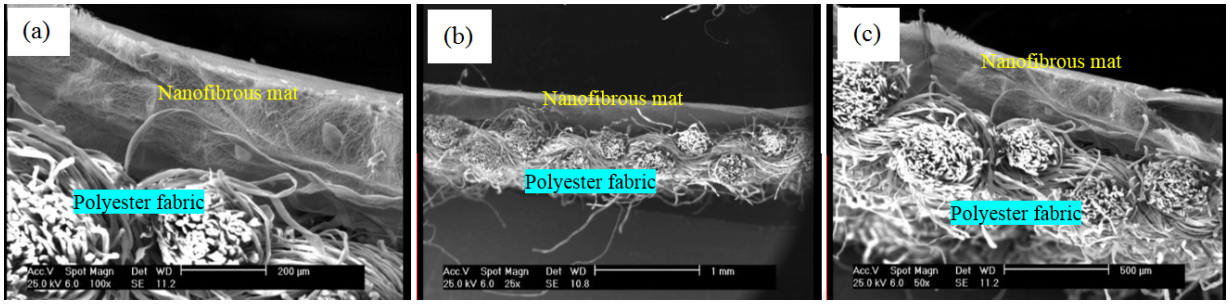

Figure 5. SEM images of the cross sections in the cross-linked PVA/PVP/Pramipexole nanofibers on the fabric, (a) 200 µm, (b) 1 mm, and (c) 500 µm magnification.

[43]. For this purpose, nanofibrous mats were immersed in PBS solution for 20 min, 6, 24 and 48 h. As shown in Fig. 6, the results show that the fibrous structure of uncross-linked PVA/PVP/Pramipexole nanofibers were disappeared by absorption of solution in the initial hours. However, the fibrous morphology of cross-linked PVA/PVP/Pramipexole mats remained stable and unchanged with porous structure until 48 h.

Atomic force microscopy (AFM) was employed to further investigate the surface morphology and topographical features of the electrospun nanofibrous mats at the nanoscale. Unlike SEM, AFM provides three-dimensional surface visualization and enables detailed observation of fiber arrangement, surface continuity, and morphological uniformity without the need for conductive coating. Representative AFM images (figure 7) reveal a continuous and interconnected nanofibrous network with uniform surface morphology, confirming the preservation of fiber integrity after electrospinning and glutaraldehyde vapor-phase cross-linking. The absence of surface cracks, collapsed regions, or fused fibers indicates that the cross-linking process did not adversely affect the nanofibrous architecture.

Subsequently, the structural characteristics and interactions of the nanofibers were examined using FTIR spectroscopy. Figure 8 (a-h) presents the FTIR spectrum of the synthesized nanofibers. The PVA nanofibers (Fig. 8 (a)) exhibited absorption bands at approximately 813, 1085, 1226, 1353, 1535, 1724, 2875, and 3614 cm^{-1}, corresponding to C–C, C–O, C–H, CH–OAC, C=O, CH_2, and –OH vibrations, respectively. Furthermore, a broad stretching band observed between 3400 and 3700 cm^{-1} was attributed to the –OH groups in PVA. The FTIR spectrum of pramipexole (Fig. 8 (h)) showed characteristic absorption bands at 839 – 945 cm^{-1} and 756 cm^{-1}, representing C–N and C–H bending vibrations. Additional distinct peaks were observed at 1253, 1575, 1599, 1714, and 2924 cm^{-1}, which were assigned to C–H stretching, N–H vibrations, the phenylnitrothiazole ring, C=N stretching, and aliphatic C–H stretching, respectively. Peaks at 3063, 3037, 3695, and 3751 cm^{-1} were further associated with NH and NH_2 functional groups within the pramipexole structure. A comparative analysis of the FTIR spectra of PVA/Pramipexole nanofibers

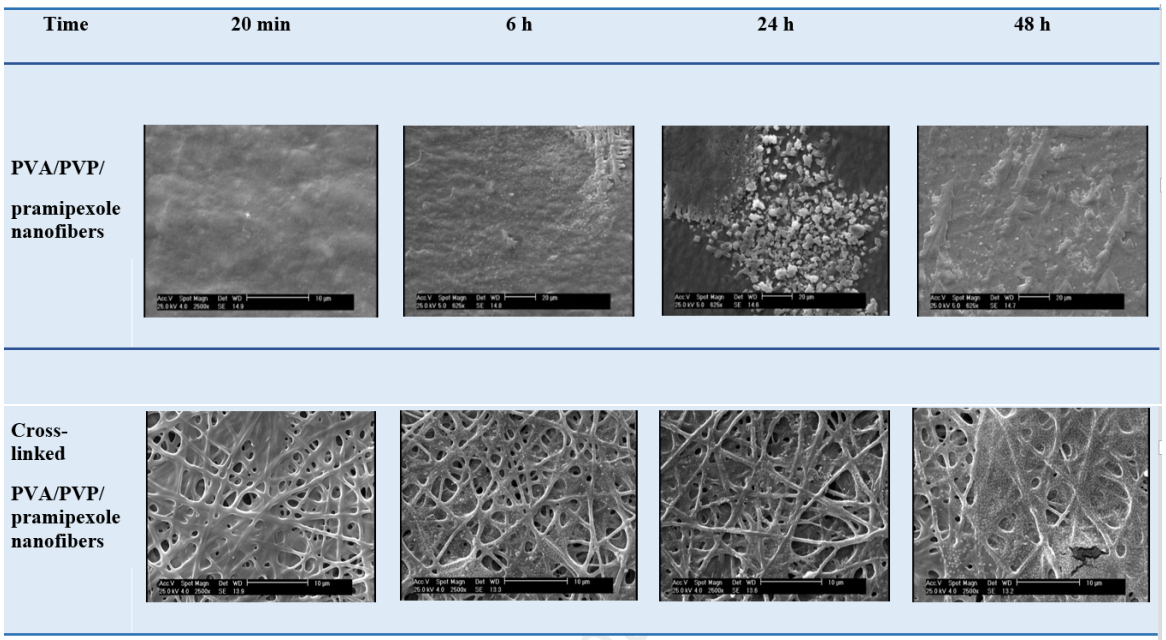

Figure 6. SEM images of PVA/PVP/Pramipexole nanofibers and cross-linked PVA/PVP/Pramipexole nanofibers in PBS solution after 20 min, 6 h, 24 h and 48 h.

https://doi.org/10.57647/ijnd.2026.1703.17

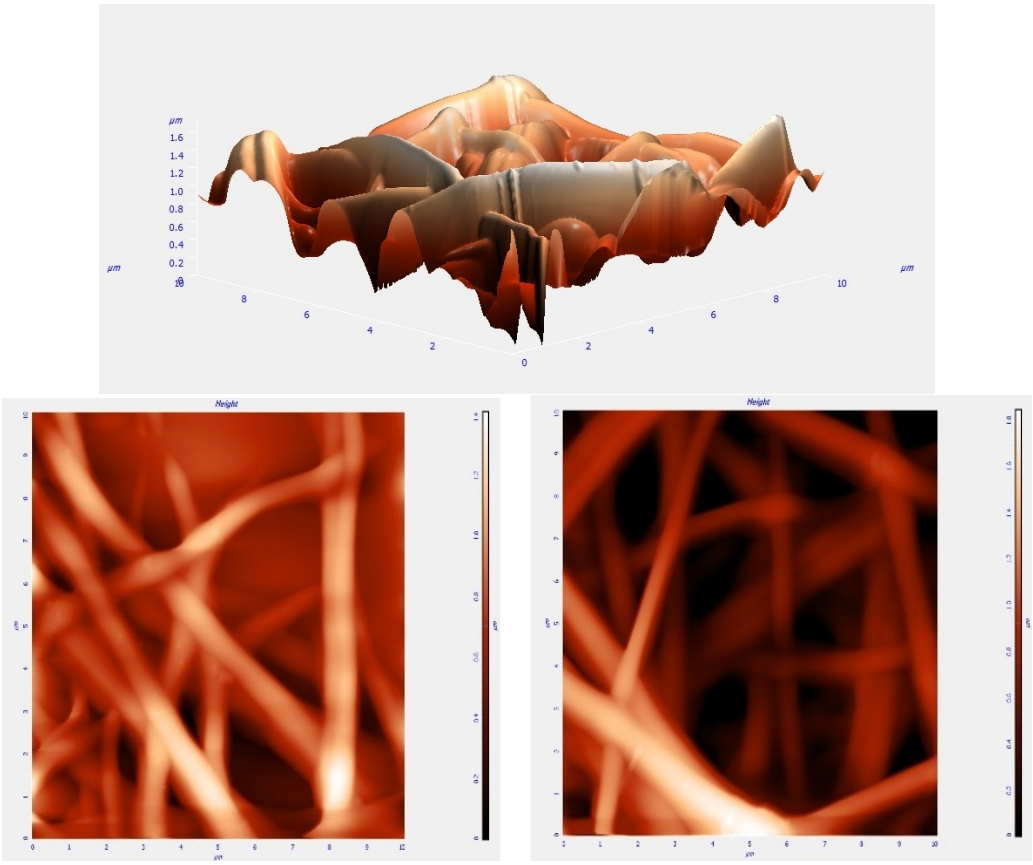

Figure 7. AFM images of the cross-linked PVA/PVP/Pramipexole nanofibers.

(Fig. 8 (d)), pure PVA nanofibers (Fig. 8 (a)), and pramipexole (Fig. 8 (h)) demonstrated that the drug incorporated into the PVA nanofibers successfully. This confirms the drug structural stability during the electrospinning process, with no signs of decomposition, hydrolysis, or structural degradation. Moreover, the comparison of the cross-linked and non-cross-linked PVA/Pramipexole nanofibers (Fig. 8 (d,f)) demonstrated similar absorption peaks to the PVA nanofibers, PVA/Pramipexole nanofibers and drug which confirmed the incorporation of PVA and drug in the cross-linked nanofibers, no structural destruction and non-degradation of the drug after cross-linking. After deshielding, peaks were observed from 1263 cm^{-1} to 1255 cm^{-1}, as well as clearer peaks at 3749 and 3854 cm^{-1}, and a broadening of the C–O band, which confirmed the crosslinking by glutaraldehyde. Figure 8 (b) presents the Fourier transform infrared (FTIR) spectrum of PVP nanofibers, highlighting distinct absorption bands at 1287, 1662, and 1423 cm^{-1}, which correspond to C–N, CH_2, and C=O stretching vibrations, respectively. A comparison between the FTIR spectra of PVA/PVP nanofibers (Fig. 8 (c)) and those of pure PVA and PVP confirmed that both polymers are retained in the blended fibers, demonstrating their stability throughout the blending and electrospinning processes. Additionally, the FTIR analysis of pramipexole and PVA/PVP/Pramipexole nanofibers revealed prominent peaks at 759, 829, 947, 1143, 1244, 1261, 1599, 1714, 2854, and 2926 cm^{-1}, confirming that pramipexole maintained its structural integrity within the electrospun nanofiber mats. FTIR analysis of the cross-linked PVA/PVP/Pramipexole nanofibers (Fig. 8 (g)) also confirmed the presence of PVA, PVP and pramipexole, with an additional broad peak at 1247 cm^{-1} attributed to O-C-O stretching, confirming the success of the cross-linking process.

As indicated in Fig. 8, all the drug-loaded nanofibers represented characteristic peaks of the drug; furthermore, no appearance of new absorption peaks was observed, which means that no chemical interactions have occurred between the drug and the polymers. It can be seen that additional proposed hydrogen bonding between polymers (PVA and PVP) and drug molecules is given in Fig. 8. Results indicated the formation of hydrogen bonding between the drug and polymers used for the preparation of nanofibers.

3.2 Water contact angle and viscosity

In order to evaluate the wettability and water penetration behavior of nanofibers, the contact angle test was performed on the solid surface of mats to determine the angle of water droplet. Figure 9 shows the contact angle of PVA, PVA/PVP and cross-linked PVA/PVP/Pramipexole nanofibers. The contact angle of electrospun PVA, PVA/PVP and cross-linked PVA/PVP nanofibers were estimated 33°, 71° and 43°, respectively. The contact angle of electrospun PVA nanofibers (Fig. 9 (a)) was determined 33° which confirms the hydrophilic feature of

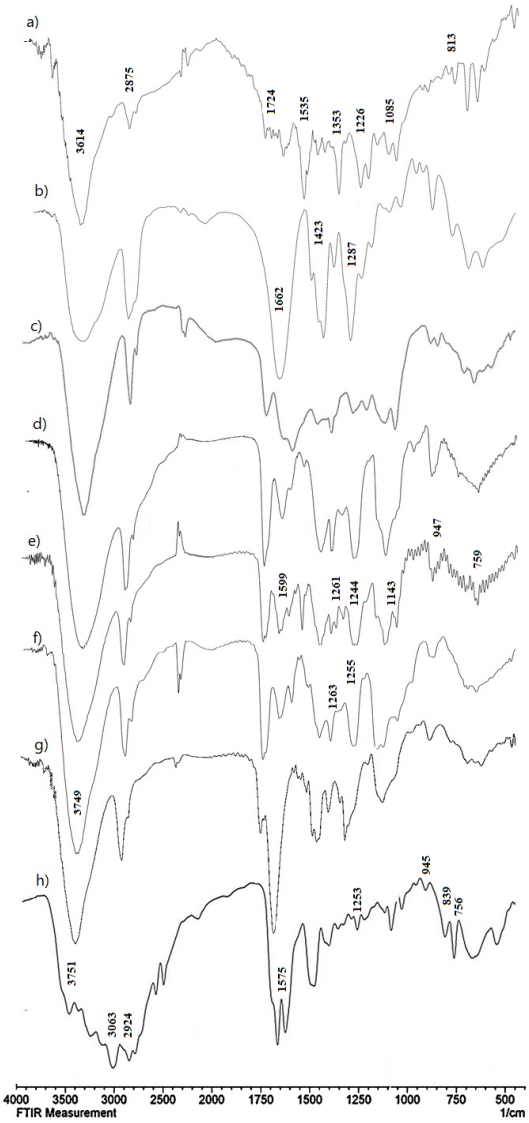

Figure 8. Fourier transform infrared (FT-IR) spectra of the nanofibers. (a) PVA nanofibers, (b) PVP nanofibers, (c) PVA/PVP nanofibers, (d) PVA/Pramipexole nanofibers, (e) PVA/PVP/Pramipexole nanofibers, (f) Cross-linked PVA/Pramipexole nanofibers, (g) Cross-linked PVA/PVP/Pramipexole nanofibers, (h) Pramipexole.

nanofibers. This medium level of wettability is suitable for use on the skin because 100% hydrophilic surface on the skin quickly absorbs water and disappears and prevents drug release, while a medium level of wettability causes slow absorption of water and drug release. The contact angle of PVA/PVP nanofibers, shown in Fig. 9 (b), was estimated 71°, which is higher than the contact angle measured in PVA nanofibers. Although the angle is less than 90 degrees and is in the medium range, which indicates the hydrophilicity of the sample, by increasing PVP content, the hydrophobicity of the sample has increased compared to PVA nanofibers. Because PVP has lower polarity and hydrophilicity, and its addition to PVA solution caused the overall decrease in hydrophilicity. Moreover, the contact angle of droplet with cross-linked PVA/PVP/Pramipexole was reported 43° indicating the hydrophilic nature of the cross-linked mats due to the higher hydrophilicity and the polarity of the pramipexole molecule (Fig. 9 (c)).

The water contact angle values obtained in this study are in good agreement with those reported for similar electrospun polymeric nanofibers in the literature. Pure electrospun PVA nanofibers tend to exhibit pronounced hydrophilicity due to the abundant hydroxyl groups in PVA, with contact angles well below 90°, consistent with previously published studies reporting PVA electrospun mats with contact angles in the range of approximately 40 – 80° depending on composition and processing conditions [44]. In blended systems, the incorporation of PVP has been shown to modify wettability. For example, electrospun PVP/PVA nanofiber mats exhibited contact angles around ~ 71°, indicating moderate hydrophilicity suitable for transdermal delivery applications, similar to our measured value for PVA/PVP nanofibers [45]. These findings are corroborated by additional reports in which PVP/PVA composite scaffolds exhibited contact angle values below 90°, reflecting retained hydrophilic character despite polymer blending, which is often attributed to the hydrophilic functional groups of both PVA and PVP that facilitate water spreading on the surface [46].

Notably, the decrease in contact angle observed for the cross-linked PVA/PVP/Pramipexole mats (43°) further aligns with expectations for systems containing hydrophilic drug molecules such as pramipexole, whose polarity can enhance surface wettability compared to the polymer blend alone. The observed hydrophilic behavior (contact angles < 90°) across all samples confirms the suitability of these nanofibrous mats for biomedical applications, particularly in transdermal drug delivery systems where controlled interaction with moisture and skin hydration is critical [47, 48].

The viscosity measurement was performed using a rotational viscometer equipped with spindle No. 42 over a shear rate range of 5 – 100 rpm. The relationship between solution viscosity and shear rate is presented in Fig. 10 (a,b,c). As observed, all solutions exhibited non-Newtonian pseudoplastic behavior, characterized by a decrease in viscosity with increasing shear rate. This shear-thinning behavior is particularly advantageous for electrospinning, as it ensures sufficient viscosity and chain entanglement at low shear rates while allowing smooth flow through the spinneret under high shear conditions. Although the viscosity curves were obtained over different shear-rate ranges for each formulation, representative viscosity values were extracted from the operational shear-rate region relevant to stable electrospinning. For the PVA/Pramipexole solution, a viscosity of approximately 65 Pa.s was observed at a shear rate of 21 rpm, whereas the PVA/PVP solution exhibited a higher viscosity of about 94 Pa.s at 190 rpm. Notably, the PVA/PVP/Pramipexole formulation showed the highest viscosity, reaching approximately 120 Pa.s at a shear rate of 106 rpm. These values clearly demonstrate the progressive increase in solution viscosity upon the incorporation of PVP and pramipexole, which can be attributed to enhanced intermolecular interactions and increased polymer chain entanglement within the

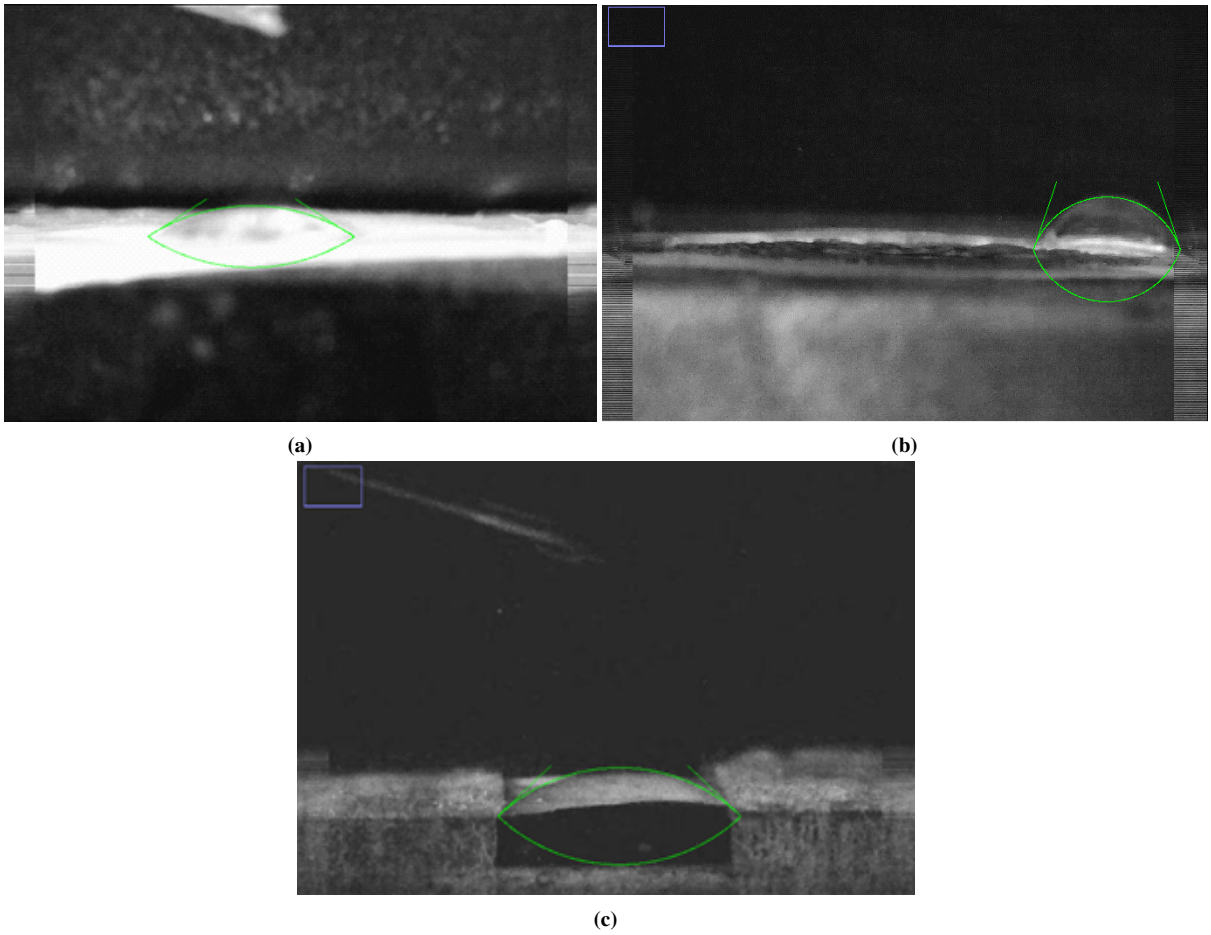

Figure 9. The contact angle of (a) PVA nanofibers, (b) PVA/PVP nanofibers, and (c) Cross-linked PVA/PVP/Pramipexole nanofibers.

solution. Higher viscosity solutions promote the formation of a stable and continuous electrospinning jet, while insufficient viscosity often leads to jet breakup or bead formation [49]. Consistent with this behavior, all fabricated nanofibers were bead-free, confirming that the viscosity of the prepared solutions was within an optimal range for electrospinning.

3.3 *In vitro* drug release

The *in vitro* release profiles of pramipexole from PVA, PVA/PVP, and glutaraldehyde vapor cross-linked PVA/PVP nanofibers were investigated in phosphate buffer solution (PBS, pH 7.4) at 37 °C over 48 h (Fig. 11). All formulations exhibited an initial burst release followed by a sustained release phase, which is a commonly observed biphasic release pattern in electrospun drug delivery systems due to rapid dissolution of surface-accessible drug followed by slower diffusion through the polymer matrix. This behavior has been reported in a wide range of polymeric electrospun fibers where the initial burst is attributed to drug molecules residing near or on the fiber surface, while the subsequent release is governed by diffusion and polymer network characteristics [50, 51, 52].

The PVA/Pramipexole nanofibers showed a pronounced burst release (~ 43% within 30 min) and reached ~ 52% cumulative release within 24 h. PVA/PVP nanofibers also exhibited an early burst (~ 32% within 30 min) followed by slower release reaching ~ 49% at 24 h. In contrast, the cross-linked PVA/PVP/Pramipexole fibers displayed a significantly slower and more sustained release profile throughout the study period. This retardation of drug release in cross-linked samples is consistent with previous reports where crosslinking of electrospun fibers reduced release rates by creating a denser polymer network, which increases the diffusion path length for drug molecules and limits polymer swelling and water uptake [53].

Mechanistically, crosslinking introduces covalent bridges between polymer chains (via glutaraldehyde reacting with hydroxyl groups of PVA/PVP), which enhances structural integrity and reduces polymer chain mobility. This effect results in reduced swelling and slower penetration of the dissolution medium, thereby decreasing drug diffusivity relative to non-cross-linked fibers. Similar findings have been observed in cross-linked PVA fibers loaded with rifampicin and isoniazid, where crosslinking reduced the release rate significantly compared to non-cross-linked counterparts, attributed to restricted chain mobility and reduced free volume within the network [54, 55]. Furthermore, the influence of crosslinking on release kinetics can be contextualized within the broader field of nanofiber drug carriers. For example, electrospun core–shell and multilayer structures,

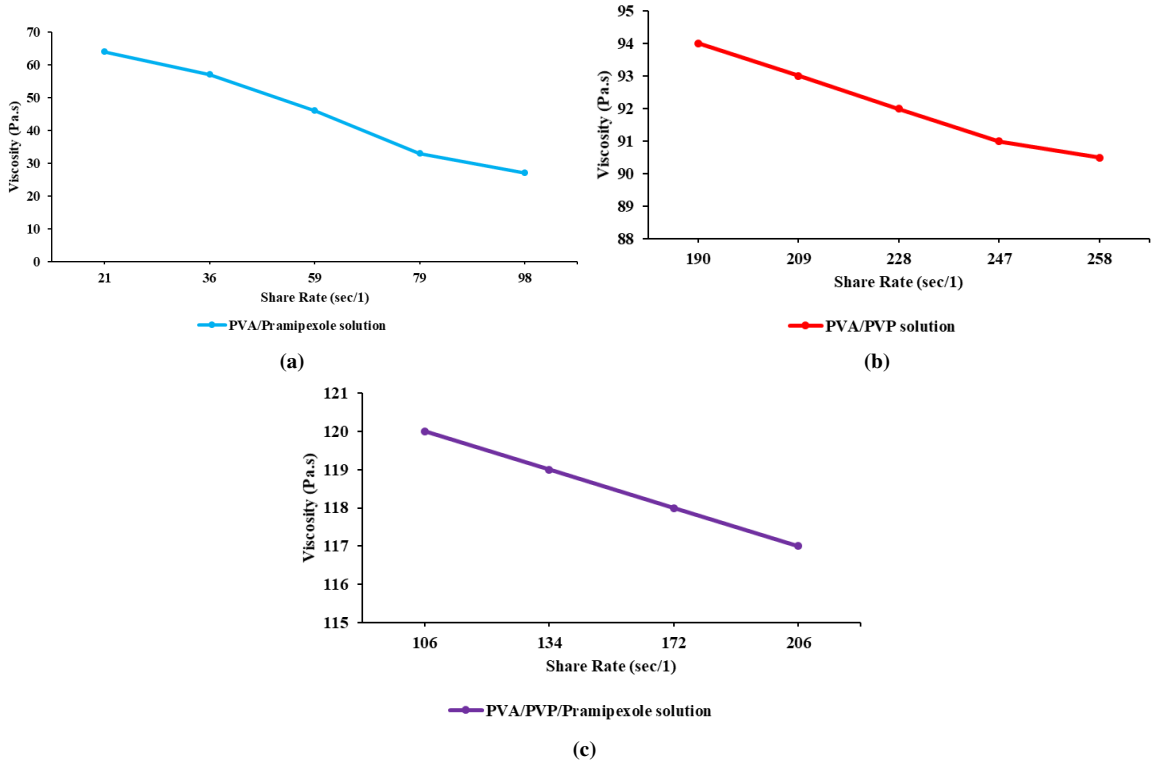

Figure 10. The viscosity graphs versus shear rate for the solutions (a) PVA/Pramipexole solution, (b) PVA/PVP solution, and (c) PVA/PVP/Pramipexole solution.

as well as polymer crosslinking, have been employed to achieve controlled, sustained release in systems such as PCL/gelatin and gelatin meshes, where enhanced diffusion barriers and network densification contributed to prolonged release profiles [56]. These strategies collectively underscore the role of physical and chemical network architecture in modulating release behavior [57, 58].

3.4 Pharmacological result

Behavioral investigations

Parkinson's disease is a common neurodegenerative condition that primarily impacts older adults, leading to both motor and non-motor impairments. Research indicates that, in patients with Parkinson's disease, the blood-brain barrier generally remains intact [59]. To fully understand the motor and behavioral implications associated to parkinsonism, our current research is focused on the sub-

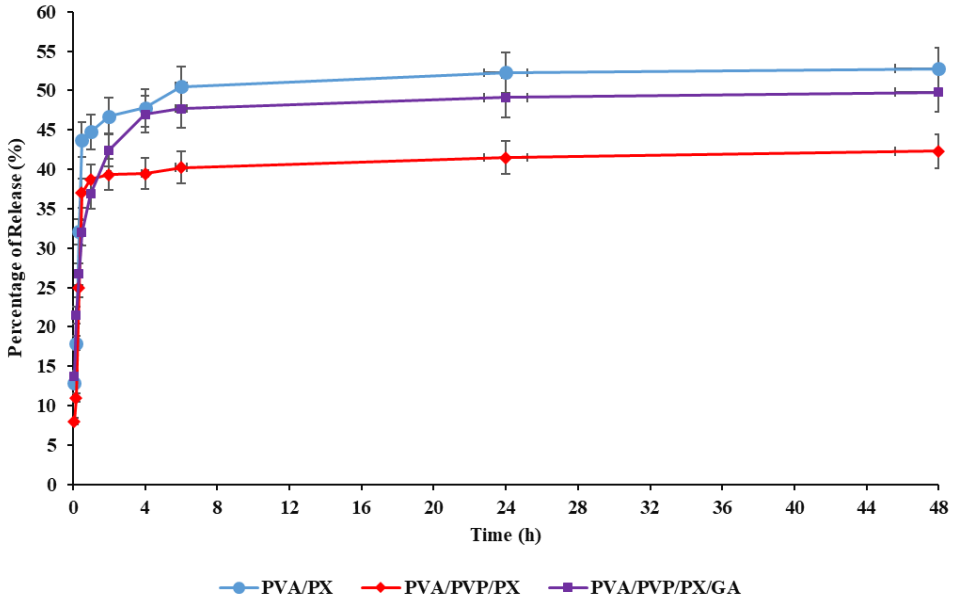

Figure 11. Drug release profiles of PVA/PX, PVA/PVP/PX and cross-linked PVA/PVP/PX nanofibers.

https://doi.org/10.57647/ijnd.2026.1703.17

stantia nigra region. The level of dopaminergic activity is closely associated with open field activity. Peripheral square crossing serves as an indicator of overall motor performance and the animal's attempt to adapt to the environment. However, central square crossings are an index of exploratory behavior [60].

The Fig. 12 (a) represents a comparison of the level of locomotor activity among the control group, paraquat-receiving group, paraquat and pramipexole-receiving group (S: systemic), and paraquat and pramipexole group-receiving (T: transdermal) in an open-field apparatus. Statistical analysis revealed that the average time and number of movements in the paraquat-treated group reduced compared to the control group. The groups receiving pramipexole, both systemically and transdermally, showed a higher number of movements, indicating the positive therapeutic effects of pramipexole skin patches and improvement in bradykinesia. Additionally, as can be seen, the treatment outcomes were the same with no significant difference between the group treated transdermally and the group treated systemically with pramipexole. The Rotarod test is extensively employed to detect impairments in motor coordination in rodent models of Parkinson's disease [61]. The obtained result of Rotarod test is shown in the Fig. 12 (b). Statistical analysis among the studied groups revealed that motor balance significantly dropped in the paraquat-receiving group versus the control group. However, in the treatment groups with systemic and transdermal pramipexole, motor balance was almost restored to the level of the control group. This indicates that transdermal pramipexole has a similar effectiveness to systemic pramipexole in improving motor balance. There was no statistically substantial difference observed between the treatment group receiving transdermal pramipexole and the group treated with systemic pramipexole.

One of the prominent indications of motor system disorder in Parkinson's disease is catalepsy, which is characterized by a hunched-back posture. The measurement of catalepsy in rats is conducted by the bar test and the results obtained from this test might be influenced by the contribution of several factors. These factors include the dimensions (diameter and height) of the bar, the method of data representation (absolute descent latency or a relative-scale), and the concept of descent latency (whether it considers the descent of a single paw or both paws off the bar). These aspects were previously discussed by Balsara et al. [62].

The comparison of latency in initiating exploratory movements using the bar test technique is shown in Fig. 12 (c). The analysis determined that the control group quickly started exploratory movements, whereas the paraquat-receiving group had a delay in the initiation of exploratory movements. However, the groups treated with pramipexole systematically and transdermally showed a decrease in this latency, which indicated the effective therapeutic impacts of transdermal pramipexole. There was no statistically significant difference observed between the treatment group receiving transdermal pramipexole and the group treated with systemic pramipexole.

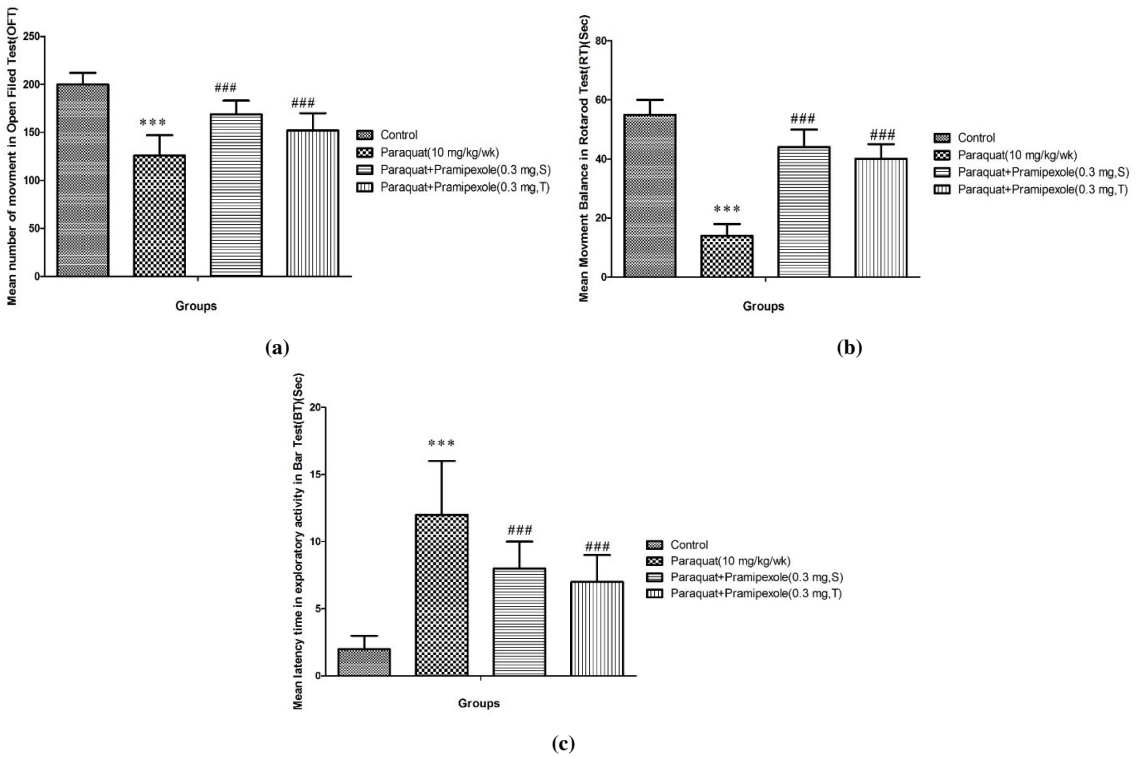

Figure 12. Depicts the average number of movements in the open-field apparatus, (a) The movement balance in Rotarod test, (b) The delay time in the start of exploratory movements in bar test, (c) ***: Significantly different from the control group at $p < 0.05$. ###: Significantly different from the paraquat group at $p < 0.05$.

https://doi.org/10.57647/ijnd.2026.1703.17

3.5 Biochemical assessment

The Brain Oxidative Stress Markers

The administration of paraquat caused a notable increase in the brain striatal MDA, which serves as an indicator for lipid peroxidation as illustrated in Fig. 13 (a,b,c,d). Furthermore, it lowered the activities of antioxidant enzymes among the target enzymes SOD (Fig. 13 (b)), GPX (Fig. 13 (c)), and GR (Fig. 13 (d)) towards the control group. The results were indicative of the fact that paraquat induced oxidative stress among the brain striatum. However, the utilization of pramipexole through both transdermal and systemic approaches exhibited a significant reduction in MDA levels (Fig. 13 (a)), while simultaneously leading to a considerable enhancement in the activity of antioxidant enzymes SOD, GPX, and GR, when compared to the Paraquat receiving group. The results indicate that the Nano fibrous patch as a treatment strategy is able to alleviate brain striatal oxidative stress in the same way as the systemic treatment does.

Oxidative stress is the result of an imbalance between systemic manifestations of reactive oxygen species and antioxidant factors. Therefore, oxidative stress contributes to many neurodegenerative diseases such as Parkinson's disease. Malondialdehyde (MDA) is one of the biomarkers of oxidative stress in the body, indicating the degree of lipid peroxidation in cells. MDA levels are anticipated to rise in the group exposed to paraquat, whereas the groups receiving pramipexole treatment both systemic and transdermal are expected to show a reduction in MDA levels. Furthermore, the present study's statistical results showed that the levels of antioxidant enzymes superoxide dismutase (SOD), glutathione peroxidase (GPx), and glutathione reductase (GR) decreased in the paraquat group compared to the control group, and increased in the systemic treatment groups with pramipexole and transdermal compared to the paraquat group. The results of previous studies also support the findings of the current study.

The Brain Inflammatory Mediators

Figure 14 illustrates that the utilization of Paraquat significantly increases TNF-α and IL1β levels within the brain striatum in contrast to the control group. This indicates that the use of paraquat has an effect of intensifying the presence of the inflammatory substances in the brain striatum. However, with the administration of pramipexole either through transdermal application or systemically, there was a tremendous reduction in TNF-α (Fig. 14 (a)) and IL1β (Fig. 14 (b)) levels in the brain striatum when contrasted to the Paraquat receiving group. It confirms that the application of nanofibers containing pramipexole has the potential to mitigate the presence of inflammatory substances in the brain striatum, similar to the effects seen in the group treated systemically.

The Apoptotic Marker

The molecular studies, depicted in figure 15, revealed significant changes in the levels of Bax (a pro-apoptotic protein) a protein that promotes cell death, and Bcl-2 (an anti-apoptotic protein) a protein that inhibits cell death, between the Paraquat group and the control group. The

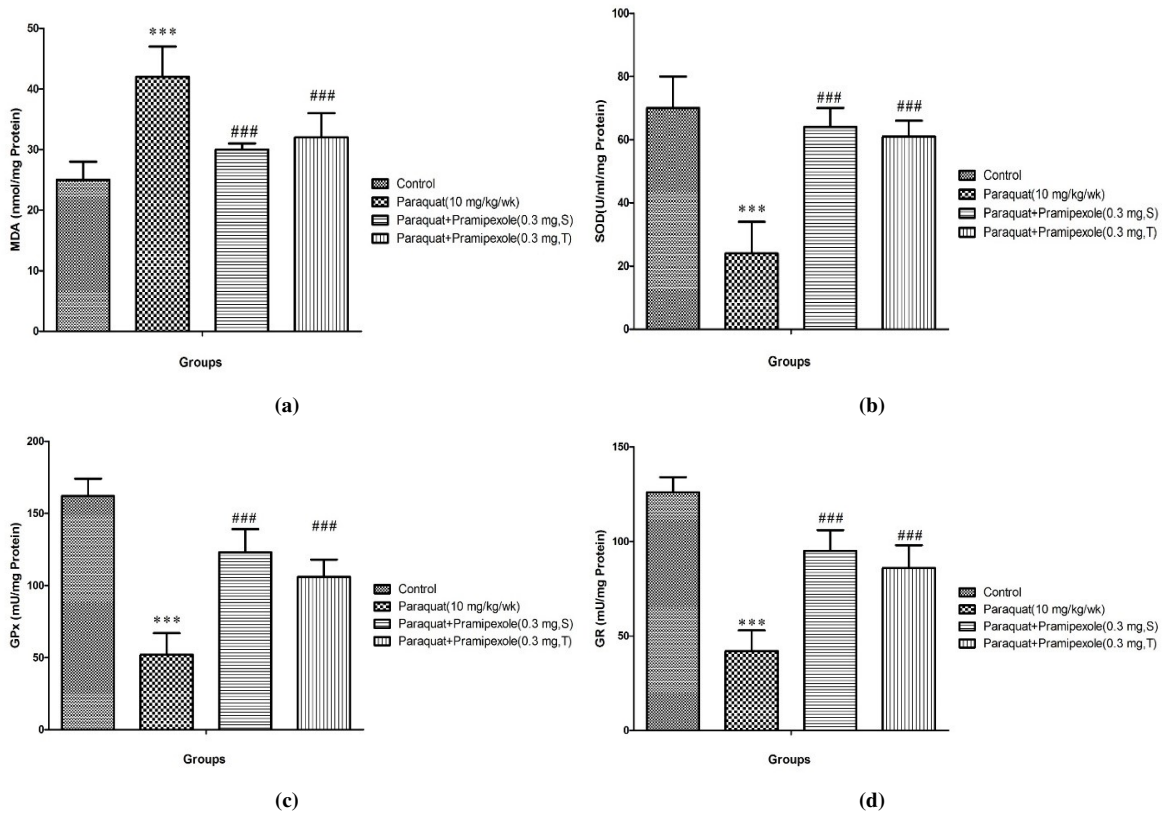

Figure 13. Effects of transdermal and systematic treatment on the content of MDA (a), and activity of SOD (b), GPX (c), and GR (d). ***: Significantly different from the control group at $p < 0.001$. ###: Significantly different from the paraquat group at $p < 0.001$.

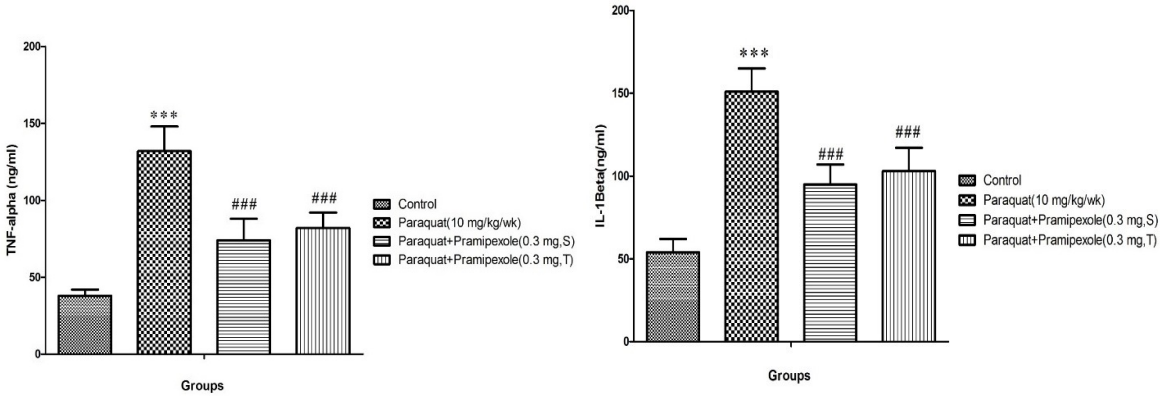

(a) **(b)**

Figure 14. Effects of transdermal and systematic treatment on the content of TNF-α (a), and IL1β (b). ***: Significantly different from the control group at $p < 0.001$. ###: Significantly different from the paraquat group at $p < 0.001$.

Paraquat-receiving group exhibited a significant increase in Bax (Fig. 15 (a)) and a significant decrease in Bcl-2 (Fig. 15 (b)). The groups treated with Pramipexole systemic and Transdermal showed a significantly lower Bax level and a significantly higher level of Bcl-2 compared to the Paraquat group. This observation is indicative of improvement in apoptosis and cell death. The ratio of pro-apoptotic and anti-apoptotic factors (Bax/Bcl-2), determines the pathway between apoptosis and cell survival [63].

In Fig. 15 (c), the statistical results indicate a substantial rise in the Bax/Bcl-2 ratio in the Paraquat-receiving group compared to the control group, indicating an increase level of pro-apoptotic factors relative to anti-apoptotic factors. while, the groups treated with Pramipexole systemic and Transdermal show a marked decrease in the Bax/Bcl-2 ratio compared to the Paraquat-receiving group, indicating a reduced level of pro-apoptotic factors and an increased level of anti-apoptotic factors.

3.6 Histopathological findings

Histopathological examination of brain tissues was performed using light microscopy at 200× magnification, focusing on the substantia nigra region (figure 16). In the control group (Fig. 16 (a)), neurons exhibited nor-

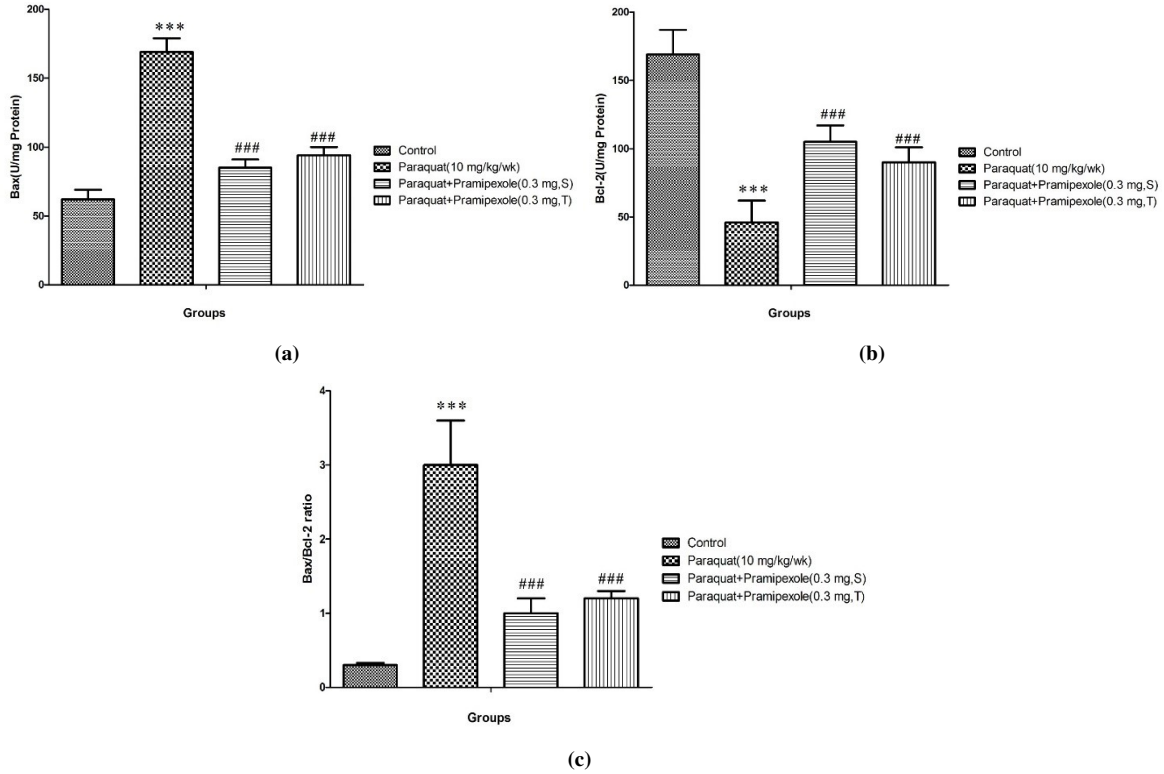

(a) **(b)**

(c)

Figure 15. Shows the amount of Bax (a) Bcl-2 (b) and Bax/Bcl-2 (c) in substantia nigra. ***: Significantly different from the control group at $p < 0.001$. ###: Significantly different from the paraquat group at $p < 0.001$.

mal morphology with intact cellular architecture, clearly defined nuclei, and absence of vacuolization or degenerative changes. In contrast, brain sections from the paraquat-treated group (Fig. 16 (b)) showed pronounced neurodegenerative alterations, including cytoplasmic vacuolization, neuronal shrinkage, and darkly stained (pyknotic) nuclei surrounded by pericellular white spaces. These features are characteristic indicators of neuronal damage and cell death associated with oxidative stress and dopaminergic neuron degeneration in Parkinsonism. Treatment with pramipexole, both via systemic administration and transdermal delivery (Fig. 16 (c,d), respectively), resulted in a marked reduction in histopathological damage compared to the paraquat group. Specifically, the number of vacuolated neurons and pyknotic nuclei was significantly decreased, and the overall cellular morphology appeared more preserved. The arrows in figure 16 highlight representative pathological features, including vacuolated neurons and pyknotic nuclei, allowing clearer comparison between untreated and treated groups. These histopathological findings are consistent with the behavioral improvements observed in the rotarod and open-field tests and support the neuroprotective effect of pramipexole against paraquat-induced dopaminergic neurodegeneration. Similar morphological changes in the substantia nigra following oxidative stress-induced Parkinsonism have been reported previously by Teema et al. [64], Ren et al. [65], and Singh et al. [66].

A number of studies, demonstrated that the pathogenesis of Parkinson disease can be rooted in both genetic predisposition and exposure to environmental neurotoxins [67, 68, 69]. In this respect, a variety of environmental exposures, such as metals, solvents, carbon monoxide, herbicides, are suspected of being causally related to Parkinson disease. Among them, the herbicide paraquat exerts typical centrally acting neurotoxic effects. Paraquat can diffuse into the CNS via neutral amino acid transporters at the blood-brain barrier, and in mouse models it selectively damages the neurons of the substantia nigra [70, 71]. The results indicated that Parkinson's disease symptoms in paraquat-induced rats were considerably improved based on the parameters used in the experiment. Since Parkinson is a slow progressive neurodegenerative disorder, we chose the paraquat-induced model of PD in rats in assessing the neuroprotective potential of pramipexole. The mechanisms underlying paraquat-induced death of dopaminergic neurons, which were provided by the redox cycling of paraquat and subsequent generation of reactive oxygen species, have been reported to mediate cell death primarily by apoptosis.

Paraquat undergoes metabolic processes through a variety of enzyme systems, including NADPH-cytochrome P450 reductase, xanthine oxidase, NADH-ubiquinone oxidoreductase, and nitric oxide synthase. This metabolism

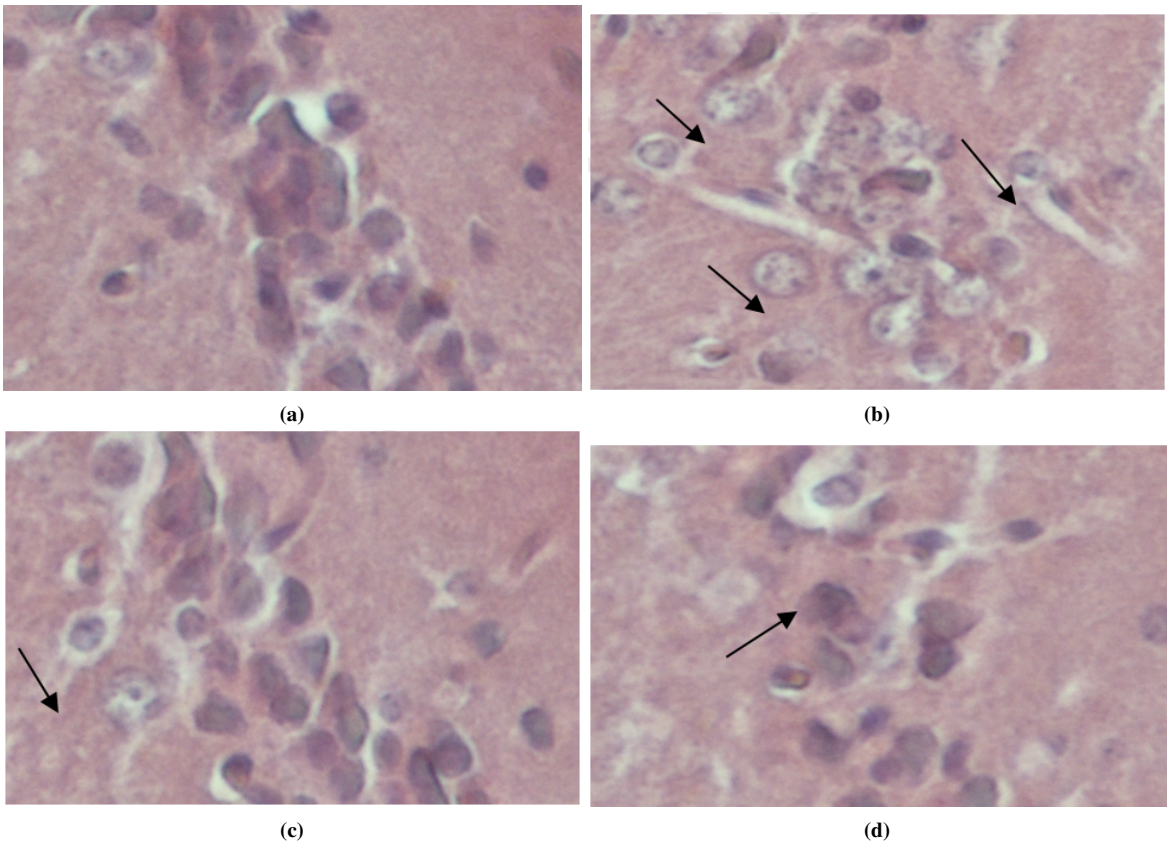

Figure 16. Histopathological images of the substantia nigra region of the brain (200× magnification): (a) Control group showing normal neuronal morphology; (b) Paraquat-treated group exhibiting vacuolated neurons and pyknotic nuclei (indicated by arrows); (c) Systemic pramipexole-treated group showing reduced neuronal degeneration; (d) Transdermal pramipexole-treated group demonstrating preserved neuronal architecture. Arrows indicate representative degenerative features such as cytoplasmic vacuolization and pyknotic nuclei.

https://doi.org/10.57647/ijnd.2026.1703.17

forms a paraquat mono-cation radical (PQ.+), which re-oxidizes to PQ2+ within the cell, forming superoxide ($O_2^{\bullet -}$). The superoxide acts as an electron acceptor and the cause of hydroxyl free radical ($HO^{\bullet}$) formation in the presence of iron, while NADP acts as an electron donor separately. These highly reactive oxygen and nitrogen species give rise to toxicity in most organs, but especially in the brain. Paraquat causes direct injury to the lining of the mouth, stomach, or intestines on contact. Upon absorption, paraquat is generally distributed and undergoes redox cycling in several tissues, especially in the liver, lungs, and kidneys, thus inducing noxious reactions of toxic chemicals. The physical symptoms resulting from brain dopaminergic neurodegeneration in PD are motor behavior impairments and are closely linked to the level of neuronal dysfunction.

Memory impairment assessment and stress-coping ability were examined with the rotarod test. The major parameter in this test is holding the rat on the spinning rod, demanding development of behavioral strategies for stress management by holding and adjusting body weight toward spinning surface. On the other hand, the paraquat-induced group showed consistent loss of behavioral activity, indicative of loss of dopaminergic neural impairment of neurons. Other activities checked included the general behavior of the rats in an open field apparatus and bar test and compared between the paraquat-induced rats and the pramipexole-treated rats. There was a remarkable improvement in walking patterns after treatment that changed the mean time and duration, indicating recovery of their coordinated motor skills for the pramipexole-treated rats. These mice had improved performances in rotarod, open field and bar tests, probably due to improved neuronal transmission resulting from reduced oxidative stress. The group treated with pramipexole using a nanofibrous patch exhibited comparable behavioral performance to the group treated with pramipexole systemically. This indicated that pramipexole was able to efficiently reduce motor deficits in Parkinson's disease, which is in concurrence with other studies. On the other hand, oxidative tension is an important element of the aging process and plays a major role in neurodegeneration. This can be attributed to the fact that the brain has the highest energy demands and consumes a large amount of oxygen but is enriched with peroxidizable polyunsaturated fatty acids. At the same time, it contains high levels of catalysts for formed reactive oxygen species, such as iron, but relatively low levels of antioxidants and related enzymes. Elevated levels of reactive oxygen species (ROS) have been linked to aging and a variety of neurodegenerative disorders associated with mitochondrial dysfunction. Oxidative stress may play a role in exacerbating mitochondrial dysfunction, or alternatively, mitochondrial impairment and oxidative stress might create a self-perpetuating cycle that intensifies both processes in neurodegenerative diseases, particularly in Parkinson's disease [72, 73]. The accumulated ROS can trigger oxidative stress and cause peroxidation damage to proteins, lipids, and nucleic acids. Superoxide dismutase and catalase are two important antioxidant enzymes that protect brain tissue from oxidative stress injury. SOD scavenges the superoxide anion radical through dismutation and converts O^{2-} into H_2O_2, which is reduced to H_2O by GPX and GR. Malondialdehyde (MDA) is considered to be a member of the group of end products of lipid peroxidation, influencing membrane fluidity and permeability, and hence a good indicator of oxidative injury [74].

In this study, paraquat induced the MDA levels and decreased the activities of SOD, GPx, and GR versus the control group. The changes were reversed by the Pramipexole nanofibrous patch. The findings indicate that the pramipexole nanofibrous patch was beneficial in mitigating paraquat-induced injury due to its strong antioxidant activity, restoring SOD, GPx, and GR activities in brain tissue. In a study conducted by Mccormak et. al, immunohistochemical analysis demonstrated that systemic administration of paraquat in Syrian mice, through oxidative pathways, leads to degeneration of dopaminergic neurons in the substantia nigra [75]. In another study, the application of topical patches containing pramipexole has been shown to decrease malondialdehyde levels and increase antioxidant enzymes, including superoxide dismutase and glutathione reductase [76]. Closely related to mitochondrial dysfunction, oxidative stress deals with a reciprocal relationship between the two. Both factors have critical roles in the pathogenesis of Parkinson's disease and are intimately associated with apoptosis [77, 78].

Bax contributes to paraquat-induced apoptosis of dopaminergic neurons, and Bcl-2 acts as a cell death inhibitor. There is an imbalance in the expression of pro-apoptotic Bax and anti-apoptotic Bcl-2 during the progression of the paraquat-induced injury in the Parkinson disease mice [79]. Our study showed that paraquat induction significantly promoted the expressions of Bax, while downregulating Bcl-2 in the striatum. The pramipexole patch partially counteracted this phenomenon. This was further supported in the study by Li et al. Pinostrobin, a potential compound possessing very strong antioxidant activity, could relieve the apoptosis caused by MPP+ exposure [80].

The Bcl-2 protein family plays an important role in the initiation of loss of cell life through the intrinsic pathway of apoptosis, which primarily involves mitochondria. Activation of pro-apoptotic proteins follows when cells get exposed to diverse cytotoxic stress, thus facilitating the release of apoptogenic factors such as the cytochrome c from the mitochondria to the cytosol. Then, the factors facilitate the activation of caspases in cytosol as an important process for initiating and performing the action of apoptosis execution [81]. Furthermore, Bax can induce apoptosis by forming homodimers or heterodimers with Bcl-2 [82].

TNF-α and IL-1β are two important cytokines known making a very significant contribution to the development of systemic inflammation, and their levels increase destroys brain cells making the body suffer from dis-

eases such as Parkinson's disease. In this research, the inflammatory factors were found to be elevated in the paraquat group compared to the control group, indicating the destruction of brain cells, while the therapeutic effects were evident in the systemic treatment groups with pramipexole and transdermal, as they showed a decrease in the levels of inflammatory factors. Furthermore, the results of other studies have shown an increase in TNF-α and IL-1β levels in the paraquat-treated group compared to the control group [83]. Another study also showed that pramipexole reduced inflammatory factors, TNF-α and IL-1β compared to the Parkinson-induced group using 6-hydroxydopamine [84].

Both behavioral and biochemical assessments revealed that the implementation of a nanofibrous patch resulted in the improvement of motor dysfunction. These results strongly suggest that the nanofibrous patch possesses the potential to provide long-term treatment for Parkinson's disease (PD). In addition, these positive outcomes were correlated with the attenuation of oxidative stress and the mitochondrial apoptosis pathway. This was evident through a decrease in malondialdehyde (MDA) levels, an increase in the activities of superoxide dismutase (SOD), glutathione peroxidase (Gpx), and glutathione reductase (GR), a reduction in tumor necrosis factor-alpha (TNF-α) and interleukin-1 beta (IL1β) levels, as well as a decrease in the Bax/Bcl-2 ratio. Considering that pramipexole, a dopamine receptor agonist, primarily acts on the striatum, we selected the substantia Nigeria as the target area to evaluate the majority of the drug's effects.

4. Conclusion

Electrospinning is a sophisticated and highly efficient method of producing ultrafine fibers from a wide range of fluids. A formulation optimized by blending PVA and PVP in a 1:1 ratio at 10% w/v was successfully developed in this study. Morphology examined that the electrospun fibrous structures of all nanofiber mats were narrow, smooth, bead free, and uniform. In addition, the statistical analysis and results for this research work prove that nanofibrous transdermal patches of pramipexole have a conclusive effect to help alleviate symptoms of motor disorders induced by paraquat in male Syrian mice, almost as effectual as the oral form of the drug. Also, the outcomes of the tissue and molecular study also validate the behavioral outcomes because pramipexole transdermal has demonstrated its efficacy to prevent cellular destruction, death, and other damages caused by paraquat-induced Parkinson's disease, to a good extent, in this way.

Acknowledgments
The authors would like to acknowledge Islamic Azad University and Razi Drug Research Center for equipment and laboratory services.

Authors contributions
All authors contributed equally to the conception, design, execution, and writing of this work. All authors read and approved the final manuscript.

Availability of data and materials
The authors declare that the data supporting the findings of this study are available within the paper.

Conflict of interests
The authors assert that they do not have any identifiable conflicting financial interests or personal relationships that might be perceived to influence the work presented in this paper.

References

1. Dzulkharnien NSF and Rohani R. "A review on current designation of metallic nanocomposite hydrogel in biomedical applications." Nanomaterials 2022; 12:1629. DOI: 10.3390/nano12101629
2. Salvador-Morales C and Grodzinski P. "Nanotechnology tools enabling biological discovery. " ACS Nano. 2022; 16:5062–84. DOI: 10.1021/acsnano.1c10635
3. Chausali N, Saxena J, and Prasad R. "Recent trends in nanotechnology applications of bio-based packaging. " J. Agric. Food Res. 2022; 7:100257. DOI: 10.1016/j.jafr.2021.100257
4. Dhanjal DS, Mehra P, Bhardwaj S, Singh R, Sharma P, Nepovimova E, et al. "Mycology-nanotechnology interface: applications in medicine and cosmetology. " Int. J. Nanomed. 2022; 17:2505–33. DOI: 10.2147/IJN.S363282
5. Pourjafari M, Ghane M, Kaboosi H, Sadeghi B, and Rezaei A. "Antibacterial Properties of Ag–Cu Alloy Nanoparticles Against Multidrug-Resistant Pseudomonas aeruginosa Through Inhibition of Quorum Sensing Pathway and Virulence-Related Genes." Journal of Biomedical Nanotechnology 2022; 18:1196–204. DOI: 10.1166/jbn.2022.3331
6. Torres-Martínez EJ, Cornejo Bravo JM, Serrano Medina A, Gonzalez GL Pérez, and Villarreal Gómez LJ. "A summary of electrospun nanofibers as drug delivery system: Drugs loaded and biopolymers used as matrices." Curr. Drug Delivery. 2018; 15:1360–74. DOI: 10.2174/1567201815666180723114326
7. Baghali M, Ziyadi H, and Faridi-Majidi R. "Fabrication and characterization of core–shell TiO_2 containing nanofbers of PCL zein by coaxial electrospinning method as an erythromycin drug carrier. " Polymer Bulletin 2022; 79:1729–49. DOI: 10.1007/s00289-021-03591-3
8. Suri SS, Fenniri H, and Singh B. "Nanotechnology-based drug delivery systems." J. Occup. Med. Toxicol. 2007; 2. DOI: 10.1186/1745-6673-2-16

9. Schätzlein AG. "Delivering cancer stem cell therapies–A role for nanomedicines." Eur. J. Cancer. 2006; 42:1309–15. DOI: 10.1016/j.ejca.2006.01.044
10. Rahmani A, Nadri S, Kazemi HS, Mortazavi Y, and Sojoodi M. "Conductive electrospun scaffolds with electrical stimulation for neural differentiation of conjunctiva mesenchymal stem cells." Artif. Organs. 2019; 43:780–90. DOI: 10.1111/aor.13425
11. Zahmatkeshan M, Adel M, Bahrami S, Esmaeili F, Rezayat SM, and Saeedi Y. "Polymer based nanofibers: preparation, fabrication, and applications. " 2018; Springer eBooks:1–47
12. Amna R, Ali K, Malik MI, and Shamsah SI. "A Brief Review of Electrospinning of Polymer Nanofibers: History and Main Applications." J. New Mater. Electrochem. Syst. 2020; 23:151–63. DOI: 10.14447/jnmes.v23i3.a01
13. Barhoum A, Pal K, Rahier H, Uludag H, Kim IS, and Bechelanya M. "Nanofibers as New-Generation Materials: From Spinning and Nano-Spinning Fabrication Techniques to Emerging Applications." Appl. Mater. Today. 2019; 17:1–35. DOI: 10.1016/j.apmt.2019.06.015
14. Li W, Peng J, Li H, Wu Z, Huang Y, Chang B, et al. "Encapsulating Nanoscale Silicon inside Carbon Fiber as Flexible Self-Supporting Anode Material for Lithium-Ion Battery. " ACS Appl Energy Mater. 2021; 4:8529–37. DOI: 10.1021/acsaem.1c01713
15. Monfared M, Taghizadeh S, Zare-Hoseinabadi A, Mousavi SM, Hashemi SA, Ranjbar S, et al. "Emerging frontiers in drug release control by core-shell nanofibers: a review. " Drug Metab. Rev. 2019; 51:589–611. DOI: 10.1080/03602532.2019.1642912
16. Hu X, Liu S, Zhou G, Huang Y, Xie Z, and Jing X. "Electrospinning of polymeric nanofibers for drug delivery applications. " J. Controlled Release. 2014; 185:12–21. DOI: 10.1016/j.jconrel.2014.04.018
17. Zamani M, Prabhakaran MP, and Ramakrishna S. "Advances in drug delivery via electrospun and electrosprayed nanomaterials. " 2013; Int. J. Nanomed. DOI: 10.2147\%2FIJN.S43575
18. Valenta C and Auner BG. "The use of polymers for dermal and transdermal delivery. " Eur. J. Pharm. Biopharm. 2004; 58:279–89. DOI: 10.1016/j.ejpb.2004.02.017
19. Mali A, Bathe RS, and Patil M. "An updated review on transdermal drug delivery systems." Int. J. of Advances in Scientific Research 2015; 1:244. DOI: 10.7439/ijasr.v1i6.2243
20. Horstink M, Tolosa E, Bonuccelli U, Deuschl G, Friedman A, et al. "Review of the therapeutic management of Parkinson's disease. Report of a joint task force of the European Federation of Neurological Societies (EFNS) and the Movement Disorder Society-European Section (MDS-ES). Part II: late (complicated) Parkinson's disease." European Journal of Neurology 2020; 13:1186–202. DOI: 10.1111/j.1468-1331.2006.01548.x
21. Lieberman A, Ranhosky A, and Korts D. "Clinical evaluation of pramipexole in advanced Parkinson's disease: results of a double-blind, placebo-controlled, parallel-group study. " Neurology 1997; 49:162–8. DOI: 10.1212/wnl.49.1.162
22. Connolly BS and Lang AE. "Pharmacological treatment of Parkinson disease: a review." Jama 2014; 311:1670. DOI: 10.1001/jama.2014.3654
23. Fawal GE, Hong H, Song X, Wu J, Sun M, et al. "Polyvinyl alcohol/hydroxyethylcellulose containing ethosomes as a scaffold for transdermal drug delivery applications." Appl. Biochem. Biotechnol. 2020; 191:1624–37. DOI: 10.1007/s12010-020-03282-1
24. Sáadon S, Razak SIA, Ismail AE, and Fakhruddin K. "Drug-loaded poly-vinyl alcohol electrospun nanofibers for transdermal drug delivery: Review on factors affecting the drug release. " Procedia Comput. Sci. 2019; 158:436–42. DOI: 10.1016/j.procs.2019.09.073
25. Sebe I, Bodai Z, Eke Z, Kallai-Szabo B, Szabo P, and Zelko R. "Comparison of directly compressed vitamin B12 tablets pre-pared from micronized rotary-spun microfibers and cast films. " Drug Dev. Ind. Pharm. 2015; 41:1438–42. DOI: 10.3109/03639045.2014.956112
26. Thenmozhi S, Dharmaraj N, Kadirvelu K, and Kim HY. "Electrospun nanofibers: New generation materials for advanced applications". Mater. Sci. Eng. B. 2017; 217:36–48. DOI: 10.1016/j.mseb.2017.01.001
27. Wang C, Ma C, Wu Z, Liang H, Yan P, Song J, Ma N, and Zhao Q. "Enhanced Bioavailability and Anticancer Effect of Curcumin-Loaded Electrospun Nanofiber: *In Vitro* and *in Vivo* Study. " Nanoscale Res. Lett. 2015; 10. DOI: https://doi.org/10.1186/s11671-015-1146-2
28. Yu DG, Zhang XF, Shen XX, Brandford-White C, and Zhu LM. "Ultrafine ibuprofen-loaded polyvinyl pyrrolidone fiber mats using electrospinning. " Polym. Int. 2009; 58:1010–3. DOI: 10.1002/pi.2629
29. Huang LY, Branford-White C, Shen XX, Yu DG, and Zhu LM. "Time-engineeringed biphasic drug release by electrospun nanofiber meshes. " Int. J. Pharm. 2012; 436:88–96. DOI: 10.1016/j.ijpharm.2012.06.058
30. Rahmani F, Ziyadi H, Baghali M, Luo H, and Ramakrishna S. "Electrospun PVP/PVA Nanofiber Mat as a Novel Potential Transdermal Drug-Delivery System for Buprenorphine: A Solution Needed for Pain Management." Appl. Sci. 11

31. Zahra F, Zhang Y, Ajayi A, Quick Q, and Mu R. "Optimization of Electrospinning Parameters for Lower Molecular Weight Polymers: A Case Study on Polyvinylpyrrolidone." Polymers 2024; 16. DOI: 10.3390/polym16091217
32. Tipduangta P, Belton P, Fábián L, Wang L, Tang H, Eddleston M, and Qi S. "Electrospun Polymer Blend Nanofibers for Tunable Drug Delivery: The Role of Transformative Phase Separation on Controlling the Release Rate." Molecular Pharmaceutics 2016; 13:25–39. DOI: 10.1021/acs.molpharmaceut.5b00359
33. Kiaka J, Moloto M, and More D. "Effect of Cellulose Acetate on the Physicochemical Properties of PVP Blended Nanofibers. " Current Nanomaterials 2025. DOI: 10.2174/0124054615358729250716131528
34. Voikar V and Stanford SC. "The Open Field Test. In book: Psychiatric Vulnerability, Mood, and Anxiety Disorders, Tests and Models in Mice and Rats." 2021 :9–29. DOI: 10.1007/978-1-0716-2748-8_2
35. Chen Y, Zhang Y, Li L, and Holscher C. "Neuroprotective effects of geniposide in the MPTP mouse model of Parkinson's disease." Eur J Pharmacol 2015; 768:21–27. DOI: 10.1016/j.ejphar.2015.09.029
36. Wadenberg ML, Soliman A, VanderSpek SC, and Kapur SC. "Dopamine D2 receptor occupancy is a common mechanism underlying animal models of antipsychotics and their clinical effects." Neuropsychopharmacology 2001; 25:633–641. DOI: 10.1016/S0893-133X(01)00261-5
37. Bancroft JD and Gamble M. "Theory and practice of histological techniques. 6th Edition". Journal of Nanomaterials 2008; Elsevier
38. Singh B, Garg T, Goyal AK, and Rath G. "Development, optimization, and characterization of polymeric electrospun nanofiber: A new attempt in sublingual delivery of nicorandil for the management of angina pectoris." Artif. Cells Nanomed. Biotechnol. 2016; 44:1498–507. DOI: 10.3109/21691401.2015.1052472
39. Ramakrishna S, Fujihara K, Teo WE, Lim TC, and Ma Z. "An Introduction to Electrospinning and Nanofibers; World Scientific Publishing Co.: Hackensack, NJ, USA." 2005
40. Chien Y, Ho M, Feng C, Yen J, Chang Y, Lai C, and Louh R. "Fabrication of Glutaraldehyde Vapor Treated PVA/SA/GO/ZnO Electrospun Nanofibers with High Liquid Absorbability for Antimicrobial of *Staphylococcus aureus*." Nanomaterials 2023; 13. DOI: 10.3390/nano13050932
41. Ullah S, Hashmi M, Hussain N, Ullah A, Sarwar M, Saito Y, Kim S, and Kim I. "Stabilized nanofibers of polyvinyl alcohol (PVA) crosslinked by unique method for efficient removal of heavy metal ions. " Journal of Water Process Engineering 2020; 33:101111. DOI: 10.1016/j.jwpe.2019.101111
42. Zhang C, Zhai T, and Turng LS. "Electrospinning of poly(lactic acid)/polycaprolactone blends: Investigation of the governing parameters and biocompatibility. " J. Polym. Eng. 2018; 38:409–17. DOI: 10.1515/polyeng-2017-0194
43. Ting-Yun K, Che-Min L, Shih-Chieh H, Tzu-Yang H, Da-Ming W, and Hsyue-Jen H. "Incorporation and selective removal of space-forming nanofibers to enhance the permeability of cytocompatible nanofiber membranes for better cell growth. " Journal of the Taiwan Institute of Chemical Engineers 2018; 91:146–54. DOI: 10.1016/j.jtice.2018.06.011
44. Doğan EE, Tokcan P, Diken ME, Yilmaz B, Kizilduman BK, and Sabaz P. "Synthesis, synthesis and some biological Properties of PVA/PVP/PN hydrogel nanocomposites: Antibacterial and biocompatibility ". Advances in Materials Sciene 2019; 19:32–45. DOI: 10.2478/adms-2019-0015
45. Rahmani F, Ziyadi H, Baghali M, Luo H, and Ramakrishna S. "Electrospun PVP/PVA Nanofiber Mat as a Novel Potential Transdermal Drug-Delivery System for Buprenorphine: A Solution Needed for Pain Management. " Applied Sciences 2021; 11:2779. DOI: 10.3390/app11062779
46. Anjum S, Li T, Arya D, Ali D, Alarifi S, Yulin W, Zhang H, Rajinikanth P, and Ao Q. "Biomimetic electrospun nanofibrous scaffold for tissue engineering: preparation, optimization by design of experiments (DOE), *in-vitro* and *in-vivo* characterization. " Frontiers in Bioengineering and Biotechnology 2023; 11. DOI: 10.3389/fbioe.2023.1288539
47. Rathore K, Singh I, Balani K, Sharma S, and Verma V. "Fabrication and characterization of multi-layered coaxial agar-based electrospun biocomposite mat, novel replacement for transdermal patches. " International Journal of Biological Macromolecules 2024 :133712. DOI: 10.1016/j.ijbiomac.2024.133712
48. Jiang Z, Zheng Z, Yu S, Gao Y, Ma J, Huang L, and Yang L. "Nanofiber Scaffolds as Drug Delivery Systems Promoting Wound Healing. " Pharmaceutics 2023; 15:1829. DOI: 10.3390/pharmaceutics15071829
49. Castkova K, Kastyl J, Sobola D, Petrus J, Stastna E, et al. "Structure–Properties Relationship of Electrospun PVDF Fibers. " Nanomaterials (Basel) 2020; 10:1221. DOI: 10.3390/nano10061221
50. Wang Y, Yu DG, Liu Y, and Liu YN. "Progress of Electrospun Nanofibrous Carriers for Modifications to Drug Release Profiles. " J Funct Biomater. 2022; 13:289. DOI: 10.3390/jfb13040289

51. Yekrang J, Gholam Shahbazi N, Rostami F, and Ramyar M. "A novel transdermal delivery route for energy supplements: Electrospun chitosan/polyvinyl alcohol nanofiber patches loaded with vitamin B12. " International Journal of Biological Macromolecules 2023; 230:123187. DOI: 10.1016/j.ijbiomac.2023.123187
52. Kamsani NH, Hasan MS, Rullah K, and Haris MS. "Nicotine-Loaded Polyvinyl Alcohol Electrospun Nanofibers as Transdermal Patches for Smoking Cessation: Formulation and Characterization. " Pharm Chem J. 2024; 57:1637–1646. DOI: 10.1007/s11094-024-03059-4
53. Shaikh RP, Kumar P, Choonara YE, du Toit LC, and Pillay V. "Crosslinked electrospun PVA nanofibrous membranes: elucidation of their physicochemical, physicomechanical and molecular disposition. " Biofabrication 2012; 4:025002. DOI: 10.1088/1758-5082/4/2/025002
54. Visser Z, Verma S, Rainey J, and Frampton J. "Loading and Release of Quercetin from Contact-Drawn Polyvinyl Alcohol Fiber Scaffolds. " ACS Pharmacology & Translational Science 2022; 5:1305–17. DOI: 10.1021/acsptsci.2c00191
55. Cui Z, Zheng Z, Lin L, Si J, Wang Q, Peng X, and Chen W. "Electrospinning and crosslinking of polyvinyl alcohol/chitosan composite nanofiber for transdermal drug delivery." Advances in Polymer Technology 2018; 37:1917–28. DOI: 10.1002/adv.21850
56. Wang Y, Yu DG, Liu Y, and Liu YN. "Progress of Electrospun Nanofibrous Carriers for Modifications to Drug Release Profiles." J. Funct. Biomater. 2022; 13:289. DOI: 10.3390/jfb13040289
57. Mehrali F, Ziyadi H, Hekmati M, Faridi-Majidi R, and Qomi M. "Electrospun kefiran biocomposite nanofibers as a novel transdermal carrier of pramipexole." Nanomedicine Research Journal 2023; 8:193–209. DOI: 10.22034/nmrj.2023.02.009
58. Moghaddami F, Yekrang J, and Dogolsar MA. "(PVA/gelatin)–(PVA/chitosan) core-sheath nanofibers as promising route for transdermal delivery of folic acid: effect of fiber morphology, folic acid dosage, and loading location on release kinetics." Emergent Mater 2025. DOI: 10.1007/s42247-025-01205-6
59. Ren Q, Ma M, Yang J, Nonaka R, Yamaguchi A, et al. "Soluble epoxide hydrolase plays a key role in the pathogenesis of Parkinson's disease." Proc Natl Acad Sci USA. 2018; 115. DOI: 10.1073/pnas.1802179115
60. Rekha KR and Selvakumar GP. "Gene expression regulation of Bcl_2, Bax and cytochrome-C by geraniol on chronic MPTP/probenecid induced C_{57}BL/6 mice model of Parkinson's disease." Chem Biol Interact. 2014; 217:57–66. DOI: 10.1016/j.cbi.2014.04.010
61. Wrangel CV, Schwabe K, John N, Krauss JK, and Alam M. "The rotenone-induced rat model of Parkinson's disease: behavioral and electrophysiological findings." Behav Brain Res. 2015; 279:52–61. DOI: 10.1016/j.bbr.2014.11.002
62. Balsara J, Jadhav J, and Chandorkar A. "Effect of drugs influencing central serotonergic mechanisms on haloperidol-induced catalepsy. " Psychopharmacology (Berl) 1979; 62:67–9. DOI: 10.1007/BF00426037
63. Oltval ZN, Milliman CL, and Korsmeyer SJ. "Bcl-2 heterodimerizes in vivo with a conserved homolog, Bax, that accelerates programmed cell death. " Cell 1993; 74:609–19. DOI: 10.1016/0092-8674(93)90509-o
64. Teema AM, Zaitone SA, and Moustafa YM. "Ibuprofen or piroxicam protects nigral neurons and delays the development of l-dopa induced dyskinesia in rats with experimental Parkinsonism: Influence on angiogenesis. " Neuropharmacology 2016; 107:432–50. DOI: 10.1016/j.neuropharm.2016.03.034
65. Ren ZI, Wang CD, Wang T, Ding H, Zhou M, Yang N, et al. "Ganoderma lucidum extract ameliorates MPTP-induced parkinsonism and protects dopaminergic neurons from oxidative stress via regulating mitochondrial function, autophagy, and apoptosis. " Acta pharmacologica Sinica 2019; 40:441–50. DOI: 10.1038/s41401-018-0077-8
66. Singh P, Hanson PS, and Morris CM. "SIRT1 ameliorates oxidative stress induced neural cell death and is down-regulated in Parkinson's disease." BMC Neuroscience 2017; 18. DOI: 10.1186/s12868-017-0364-1
67. Dinis-Oliveira RJ, Remiao F, Carmo H, Duarte JA, Navarro AS, et al. "Paraquat exposure as an etiological factor of Parkinson's disease. " Neurotoxicology 2022; 27:1110–22. DOI: 10.1016/j.neuro.2006.05.012
68. Di Monte DA. "The environment and Parkinson's disease: is the nigrostriatal system preferentially targeted by neurotoxins? " Lancet Neurol. 2003; 2:531–8. DOI: 10.1016/s1474-4422(03)00501-5
69. McCormack AL, Thiruchelvam M, Manning-Bog AB, Thiffault C, Langston JW, et al. "Environmental risk factors and Parkinson's disease: Selective degeneration of nigral dopaminergic neurons caused by the herbicide paraquat." Neurobiol Dis. 2002; 10:119–27. DOI: 10.1006/nbdi.2002.0507
70. Vanacore N, Nappo A, Gentile M, Brustolin A, Palange S, et al. "Evaluation of risk of Parkinson's disease in a cohort of licensed pesticide users." Neurol Sci. 2002; 23:s119–20. DOI: 10.1007/s100720200098

71. McCormack AL, Atienza JG, Johnston LC, Andersen JK, Vu S, and Di Monte DA. "Role of oxidative stress in paraquat-induced dopaminergic cell degeneration." J Neurochem. 2005; 93:1030–7. DOI: 10.1111/j.1471-4159.2005.03088.x

72. Dauer W and Przedborski S. "Parkinson's disease: mechanisms and models. " Neuron. 2003; 39:889–909. DOI: 10.1016/s0896-6273(03)00568-3

73. Uttara B, Singh AV, Zamboni P, and Mahajan RT. "Oxidative stress and neurodegenerative diseases: a review of upstream and downstream antioxidant therapeutic options. " Curr Neuropharmacol. 2009; 7:65–74. DOI: 10.2174\%2F157015909787602823

74. Schramm A, Matusik P, Osmenda G, and Guzik TJ. "Targeting NADPH oxidases in vascular pharmacology. " Vasc Pharmacol. 2012; 56:216–31. DOI: 10.1016/j.vph.2012.02.012

75. McCormack AL, Thiruchelvam M, Manning-Bog AB, Thiffault C, Langston JW, et al. "Environmental risk factors and Parkinson's disease: Selective degeneration of nigral dopaminergic neurons caused by the herbicide paraquat." Neurobiol Dis. 2002; 10:119–27. DOI: 10.1006/nbdi.2002.0507

76. Wang Y, Yu X, Zhang P, Ma Y, Wang L, Xu H, and Sui D. "Neuroprotective effects of pramipexole transdermal patch in the MPTP-induced mouse model of Parkinson's disease. " Journal of Pharmacological Sciences 2018; 138:31–7. DOI: 10.1016/j.jphs.2018.08.008

77. Abou-Sleiman PM, Muqit MM, and Wood NW. "Expanding insights of mitochondrial dysfunction in Parkinson's disease. " Nat Rev Neurosci. 2006; 7:207–19. DOI: 10.1038/nrn1868

78. Henchcliffe C and Beal MF. "Mitochondrial biology and oxidative stress in Parkinson disease pathogenesis. " Nat Clin Pract Neurol. 2008; 4:600–9. DOI: 10.1038/ncpneuro0924

79. Li Y, Liu W, Li L, and Holscher C. "Neuroprotective effects of a GIP analogue in the MPTP Parkinson's disease mouse model. " Neuropharmacology 2016; 101:255–63. DOI: 10.1016/j.neuropharm.2015.10.002

80. Li C, Tang B, Feng Y, et al. "Pinostrobin exerts neuroprotective actions in neurotoxin-induced Parkinson's disease models through Nrf2 induction." J Agric Food Chem. 2019; 66:8307–18. DOI: 10.1021/acs.jafc.8b02607

81. Czabotar PE, Lessene G, Strasser A, et al. "Control of apoptosis by the Bcl-2 protein family: implications for physiology and therapy." Nat Rev Mol Cell Biol. 2014; 15:49–63. DOI: 10.1038/nrm3722

82. Eleawa SM, Alkhateeb MA, Alhashem FH, et al. "Resveratrol reverses cadmium chloride-induced testicular damage and subfertility by downregulating p53 and Bax and upregulating gonadotropins and Bcl-2 gene expression. " J. Reprod Dev. 2022; 60:115–27. DOI: 10.1262/jrd.2013-097

83. Mitra S, Chakrabarti N, and Bhattacharyya A. "Differential regional expression patterns of α-synuclein, TNF-α, and IL-1β; and variable status of dopaminergic neurotoxicity in mouse brain after Paraquat treatment. " Journal of Neuroinflammation 2011; 8. DOI: 10.1186/1742-2094-8-163

84. Farbood Y, Sarkaki A, Dolatshahi M, Mansouri SMT, and Khodadadi A. "Ellagic Acid Protects the Brain Against 6-Hydroxydopamine Induced Neuroinflammation in a Rat Model of Parkinson. " Basic Clin. Neurosci. 2015; 6:83–9